

MAGNETOSHEATH INTERACTION WITH THE HIGH LATITUDE MAGNETOPAUSE

S. SAVIN¹, A. SKALSKY¹, L. ZELENYI¹, L. AVANOV¹, N. BORODKOVA¹,
S. KLIMOV¹, V. LUTSENKO¹, E. PANOV¹, S. ROMANOV¹, V. SMIRNOV¹,
YU. YERMOLAEV¹, P. SONG², E. AMATA³, G. CONSOLINI³, T. A. FRITZ⁴,
J. BUECHNER⁵, B. NIKUTOWSKI⁵, J. BLECKI⁶, C. FARRUGIA⁷,
N. MAYNARD⁸, J. PICKETT⁹, J. A. SAUVAUD¹⁰, J. L. RAUCH¹¹,
J. G. TROTIGNON¹¹, Y. KHOTYAINTEV¹² and K. STASIEWICZ¹²

¹*Space Research Institute, Profsoyuznaya 84/32, Moscow, 117810, Russia*
E-mail: ssavin@iki.rssi.ru;

²*University of Massachusetts, Lowell, MA, USA;*

³*Interplanetary Space Physics Institute, CNR, Roma, Italy;*

⁴*Boston University, Boston, MA, USA;*

⁵*Max-Planck Inst, Aeronomie, Katlenburg-Lindau, Germany;*

⁶*Space Research Center, Warsaw, Poland;*

⁷*University of New Hampshire, Durham, NH, USA;*

⁸*Mission Research Corporation, Nashua, NH, USA;*

⁹*University of Iowa, Iowa City, IA, USA;*

¹⁰*CESR, Toulouse, France;*

¹¹*LPCE, Orleans, France;*

¹²*IRF-U, Uppsala, Sweden*

(Received 9 February 2003; Accepted 30 April 2004)

Abstract. We present both statistical and case studies of magnetosheath interaction with the high-latitude magnetopause on the basis of Interball-1 and other ISTP spacecraft data. We discuss those data along with recently published results on the topology of cusp-magnetosheath transition and the roles of nonlinear disturbances in mass and energy transfer across the high-latitude magnetopause. For sunward dipole tilts, a cusp throat is magnetically open for direct interaction with the incident flow that results in the creation of a turbulent boundary layer (TBL) over an indented magnetopause and downstream of the cusp. For antisunward tilts, the cusp throat is closed by a smooth magnetopause; demagnetized ‘plasma balls’ (with scale \sim few R_E , an occurrence rate of \sim 25% and trapped energetic particles) present a major magnetosheath plasma channel just inside the cusp. The flow interacts with the ‘plasma balls’ via reflected waves, which trigger a chaotization of up to 40% of the upstream kinetic energy. These waves propagate upstream of the TBL and initiate amplification of the existing magnetosheath waves and their cascade-like decays during downstream passage throughout the TBL. The most striking feature of the nonlinear interaction is the appearance of magnetosonic jets, accelerated up to an Alfvénic Mach number of 3. The characteristic impulsive local momentum loss is followed by decelerated Alfvénic flows and modulated by the TBL waves; momentum balance is conserved only on time scales of the Alfvénic flows ($1/f_A \sim 12$ min). Wave trains at $f_A \sim 1.3$ mHz are capable of synchronizing interactions throughout the outer and inner boundary layers. The sonic/Alfvénic flows, bounded by current sheets, control the TBL

spectral shape and result in non-Gaussian statistical characteristics of the disturbances, indicating the fluctuation intermittency. We suggest that the multi-scale TBL processes play at least a comparable role to that of macro-reconnection (remote from or in the cusp) in solar wind energy transformation and population of the magnetosphere by the magnetosheath plasma. Secondary micro-reconnection constitutes a necessary chain at the small-scale (\sim ion gyroradius) edge of the TBL cascades. The thick TBL transforms the flow energy, including deceleration and heating of the flow in the open throat, ‘plasma ball’ and the region downstream of the cusp.

Keywords: boundary layer, cusp, magnetopause, magnetosheath

Abbreviations: BL – Boundary Layer; FOV – Field Of View; MP – Magnetopause; GSM – Geocentric Solar Magnetic; MSH – Magnetosheath; SW – Solar Wind; ULF – Ultra-Low Frequency; UT – Universal Time; MLT – Magnetic Local Time; HEOS – Highly Eccentric Orbiting Satellite; ISEE – International Sun-Earth Explorers; GDCF – Gas Dynamic Connected Field model; FOV – Field Of View; GSE – Geocentric Solar Ecliptic

1. Introduction

Early single spacecraft observations with Heos-2 and later Prognoz-7, 8, 10 have shown that the magnetopause (MP) position and magnetosheath plasma flow structures are quite variable near the cusp, a magnetospheric region that is crucial for magnetosheath plasma entry (Haerendel and Paschmann, 1975; Paschmann et al., 1976; Klimov et al., 1986; Savin, 1994). Haerendel (1978) first introduced the turbulent boundary layer (TBL) to cusp physics in a discussion on the interaction of the magnetosheath flow with the magnetopause at the flank of the tail lobe. We reproduce his TBL sketch in Figure 1a: a laminar hydrodynamic flow interacts with an obstacle by generation of a TBL both in front of the obstacle (marked by “1”) and behind it (marked by “2”). The zone “1” corresponds to the funnel-shaped cusp throat in Figure 1b; the obstacle is presented by uprising magnetic field tubes at the tailward cusp wall. The downstream zone “2” has been poorly studied (see Savin et al., 2004, and references therein). Because of differences in characteristics, researchers have divided the high altitude cusp into a number of layers and regions. Since full agreement in terminology is not yet achieved, we provide our definitions of the regions discussed in this paper. These regions, as shown in Figure 1b, are the outer and inner cusps, the open throat (OT) of the outer cusp, and the turbulent boundary layer. We will demonstrate, however, that the interaction pattern in Figure 1 should be further modified for winter cusp crossings.

In Figure 1b, the OT (slant-line shaded region) is outside the MP, the outer cusp (gray) is just inside the MP, and the inner cusp (black) is deeper in the magnetosphere. We identify the MP (inner white line) as the innermost current sheet where the magnetic field turns from Earth-controlled to magnetosheath-controlled (Haerendel and Paschmann, 1975). The outer cusp (OC) is a region with three different particle populations: newly injected

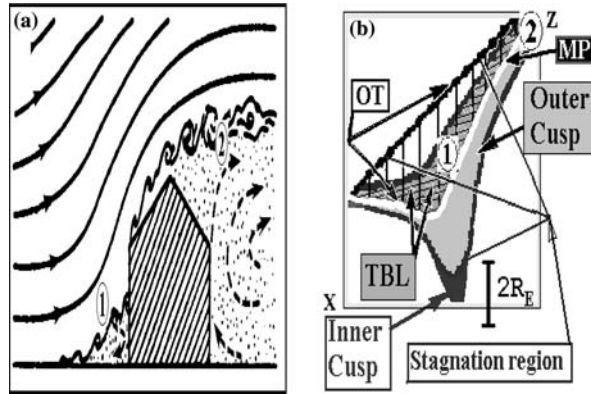


Figure 1. (a) Generation of a turbulent boundary layer in the process of interaction of hydrodynamic flow with an obstacle (from Haerendel, 1978). “1” – marks open cusp throat, “2” – stands for high latitude boundary layer downstream of the cusp. (b) Sketch for MSH/cusp interface in the noon-midnight plane from (Savin et al., 2002a). The boundaries and sub-regions are described in the text.

MSH ions, MSH ions reflected from the ionosphere, and quasi-perpendicular ions trapped in the local magnetic field minimum near the cusp (Savin et al., 1998b; Sandahl et al., 2002). There are also electrons accelerated along the field lines. The newly injected and quasi-perpendicular ions dominate over those that are reflected. This is one of the characteristics distinguishing the outer cusp from the inner cusp and from the distant mantle. The outer cusp is also characterized by moderate magnetic noise, while in the inner cusp (IC) there is a similar type of noise observed primarily only at the boundaries (Pottelette et al., 1990). The outer cusp consists of the entry layer and the portion of the plasma mantle adjoining the entry layer (Paschmann et al., 1976). According to the work of Yamauchi and Lundin (1997) the entry layer and mantle that are parts of the outer cusp form one continuous region.

At the cusp the magnetopause can be indented. This indentation was first predicted by Spreiter and Briggs (1962) and then detected by HEOS-2 (Paschmann et al., 1976), ISEE (Petrinec and Russell, 1995), and Hawkeye-1 (S. Chen et al., 1997). Interball-1 early statistics show that the indentation is on the average about $2 R_E$ deep (Savin et al., 1998b). We call this part of the exterior cusp the OT. The plasma in the OT is highly disturbed and/or stagnant MSH plasma. The turbulent boundary layer (TBL) is a region dominated by irregular magnetic fields and plasma flows. It is located just outside and/or at the near cusp magnetopause and has recently been found to be a permanent feature (Savin et al., 1997, 1998b, 2002a; Sandahl et al., 2002). Here the energy density of the ultra low frequency (ULF) fluctuations is comparable to the ion kinetic, thermal, and DC magnetic field densities. The ULF power is usually several times larger than that in the MSH, and one

or two orders of magnitude larger than that inside the magnetopause. As recent studies conclude (see, e.g., Belmont and Rezeau, 2001, and references therein), the strong ULF fluctuations that occur just outside of or at the magnetopause can independently result in micro-reconnection and local plasma penetration all along the magnetopause surface, even without the presence of quasi-stationary global reconnection. Examples of highly turbulent magnetic and electric fields in the exterior cusp have been reported by Paschmann et al. (1976) from Heos-2, by Klimov et al. (1986) from Prognoz-10, by Savin (1994) and Blecki et al. (1998) from Prognoz-8 and by S. Chen et al. (1997) from Hawkeye-1 data.

The main goal of this paper is to survey achievements in this area and explore solutions to the problems associated with the TBL and exterior cusp physics in the Interball era. The recent baseline case studies are described in detail in Savin et al. (2001, 2002a, b, 2004). An Interball-Polar case on 19 June 1998 is utilized to display the characteristic TBL features. It demonstrates the asymmetry of boundary layers for positive (sunward) Earth magnetic dipole tilts in summer and that of the negative (anti-sunward) tilts in winter. We reproduce the most interesting results from the previous studies and analyze detailed dynamics of the ion energy and of Poynting flux to clarify the pattern of nonlinear interactions in the upstream TBL. The wave packets, going from MP upstream in a subsonic MSH flow, occur to stimulate partial randomization of the flow far in front of the MP, while the SW driver plays a minor role. The interaction with the upstream going waves launches downstream-accelerated jets at about sonic speed. The jets break up the homogeneous equilibrium streamlining by carrying down-flow up to half of the flow momentum density. That signifies the cascade-like non-linear energy transformation in the TBL, proposed by Savin et al. (2001).

We present, for the first time, a full statistical review of the high level ULF magnetic turbulence (i.e. of the TBL) from the Interball-1 data, concentrating on the MP asymmetry for the summer and winter hemispheres. The permanent plasma heating in the TBL is regarded as a result of transformation of MSH flow energy into the random and thermal energies in the process of the MSH flow interaction with the outer cusp throat. We exhibit de-magnetized large-scale ‘plasma balls’ inside the winter MP and study their statistics versus that of stagnant MSH plasma outside the NP in summer. We also present 3D maps of the TBL dependence on the fluctuation power and on the dipole tilt and study the ‘plasma ball’ occurrence that depends on the tilt, magnetic shear and interplanetary magnetic field. Finally, we discuss the presented and published Interball-1 data in relation to the MSH plasma penetration and acceleration both due to plasma percolation and turbulent heating and due to multi-scale reconnection of anti-parallel magnetic fields. We address the practically unexplored interaction of MSH flow with stagnant high-beta ‘plasma ball’ via the highly super-Alfvénic jets and decelerated

Alfvén flows embedded into the coherent pattern of cascade-like interactions in the upstream TBL.

2. Turbulent boundary layer and “plasma ball” on 19 June 1998

Data from 19 June 1998 (Figure 2) illustrate the recent findings at the MSH/cusp interface. Geotail provided high-resolution SW magnetic field and synchronization with WIND plasma data, Polar traced the northern (summer) stagnation region, and Interball-1 entered the southern cusp from the MSH. The Gas Dynamic Convection model (GDCF), which is described in detail by Song et al. (1999a, b) and Dubinin et al. (2002), links the multipoint observations. While several recent papers describe some features of this event (Savin et al., 2002a, b, 2004), we report new, valuable findings in the interaction pattern.

2.1. INBOUND MAGNETOPAUSE CROSSING

We present a sketch in Figure 3 (turned upside down for easy comparison with Figure 1b) to provide a guide for a different topology on 19 June 1998 compared with that in Figure 1. The southern hemisphere MP here has no indentation. The disturbances of the ion flow in the XZ plane (‘outer BL’) start in the upstream (relative to MP) flow and result in the appearance of the accelerated jets first at ~09 UT and then in front of the MP in the tailward stream (upstream TBL). The criteria fulfilling the definition of the TBL (see Section 3) are marked by gray bars on the bottom.

In the TBL map in Figure 2.A1 this case appears as a 20 min interval, centered at ~09 UT, with the interval at 09:20–10:40 UT colored according to the D_f magnitude (black curve in Figure 2.A6i, see discussion below). The MP transition is thick and imbedded into the TBL, which terminates in a ‘plasma ball’ (PB, see Savin et al., 2002a). The PB is a high-beta (in this case up to 15) large-scale (few R_E) sub-region of the OC (Figure 3). As Savin et al. (1998b) and Kirpichev et al. (1999) have shown, the general OC (and PB) feature trapped MSH-origin ions – are often seen in low-beta and small-scale regions (i.e. the PB occurrence is much smaller than that of the OC, see Section 4). In the PB the magnetic field is reduced, marking the boundary between the dayside and mantle/polar cap magnetic field lines. The PB average position should tend to shift towards the anti-parallel magnetic field through the MP that corresponds to the place of minimal $B^2/2\mu_0$, predicted by the fields’ vector sum (cf. Spreiter and Briggs, 1962). We will refer hereafter to the OT only in the case of the configuration of Figure 1b, which seems to be characteristic for positive tilts (see Figure 2.A2–2.A4 and related discussions in Sections 3 and 4).

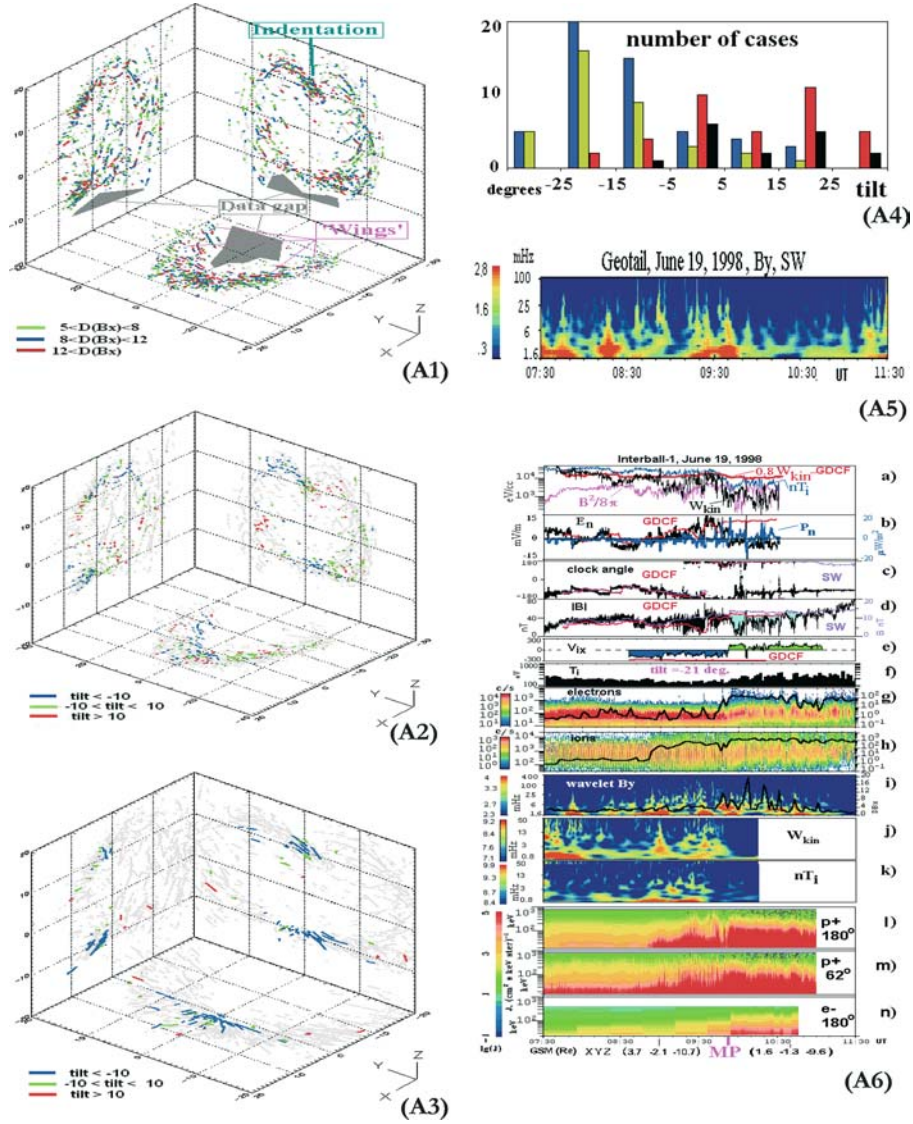


Figure 2. (A1) TBL level map (nT) in 3 GSM planes (gray color – $D(B_x) > 3 nT$). (A2) TBL tilt dependence for $D(B_x) > 8 nT$. (A3) PB tilt (degrees) dependence (gray color – TBL). (A4) Tilt dependence of PB (blue, green) and open OT. (A5) SW B_y spectrogram (Geotail) on 19 June 1998. (A6) TBL and PB on 19 June 1998. (a) energy densities; (b) normal electric field and Poynting vector; (c) magnetic clock angle; (d) $|B|$; (e) ion V_x velocity; (f) ion temperature; (g) electron spectrogram and intensity (> 30 keV); (h) ion spectrogram and intensity (> 30 keV); (i) magnetic B_y – spectrogram and B_x -variation; (j) ion kinetic energy spectrogram; (k) ion thermal energy spectrogram; (l–n) energetic ions (FOV 180 and 62 deg. from Sun) and electrons (FOV 180°. from Sun).

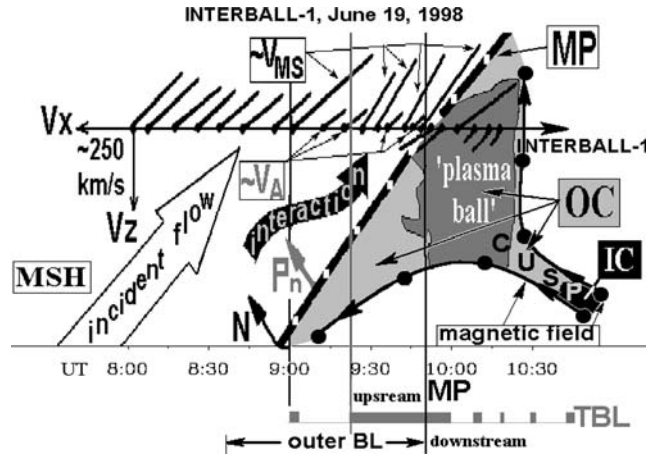


Figure 3. Sketch for the interaction pattern of MSH plasma flow with outer cusp on 19 June 1998; spacecraft orbit (Interball-1 moves from left to right), with characteristic ion velocity vectors in the XZ GSE plane; \vec{N} - normal to MP in GSE frame $\sim(0.7, 0.07, -0.71)$; P_n -projection of Poynting vector on \vec{N} ; V_{MS} , V_A -magnetosonic and Alfvén speeds, see also Figure 4; MP is shown by the thick broken curve; OC, IC – see Figure 1 and related discussions.

In Figure 3 the cusp throat is closed by the smooth MP at a larger distance, when compared with Figure 1b. A principal problem is distinguishing dynamic interactions of the SW with the MP from local disturbances. For this purpose in Figure 2.A5 a wavelet spectrogram (see details in Savin et al., 2002b) of the IMF GSE B_y -component from Geotail is shown for 1.6–100 mHz range (octave-based frequency scale in Hz and color scale for logarithm of the wave power in $[nT^2/Hz]$ are shown on the left side). We compare the Geotail data with those of Interball-1, given in panel i in Figure 2.A6, where a black line represents the B_x -variation for 2-min intervals from 4 Hz-sampling of the magnetic field (Df, scale on right side in $[nT/Hz^{1/2}]$). The MP crossing (from MSH to OC, see Figure 3) is marked at the bottom of Figure 2.A6, along with the Interball-1 position in the GSM frame at two points. In panel a of Figure 2.A6 we display energy densities in eV/cc; ion thermal nT_i (n and T_i -ion density and temperature) – blue line; DC magnetic $B^2/2\mu_0$ -violet line; kinetic energy W_{kin} -black line; the red curve presents GDCF predictions for W_{kin} , multiplied by a factor of 0.8 to adjust the measured value in the middle MSH (following Savin et al., 2004). The time lag is chosen for best fit at 08:40–09:50 UT, while it is certainly different for 07:30–08:30 UT (see Dubinin et al. (2002) and Figure 4 below).

Panel b of Figure 2.A5 shows the electric field (E_n , black line), calculated from the vector product of ion velocity and magnetic field, along the MP normal ($\vec{N} \sim (0.7, 0.07, -0.71)$ in the GSE frame (see Savin et al. 2002a, b), and that of the Poynting vector P_n at 5–50 mHz (blue line), also in the N

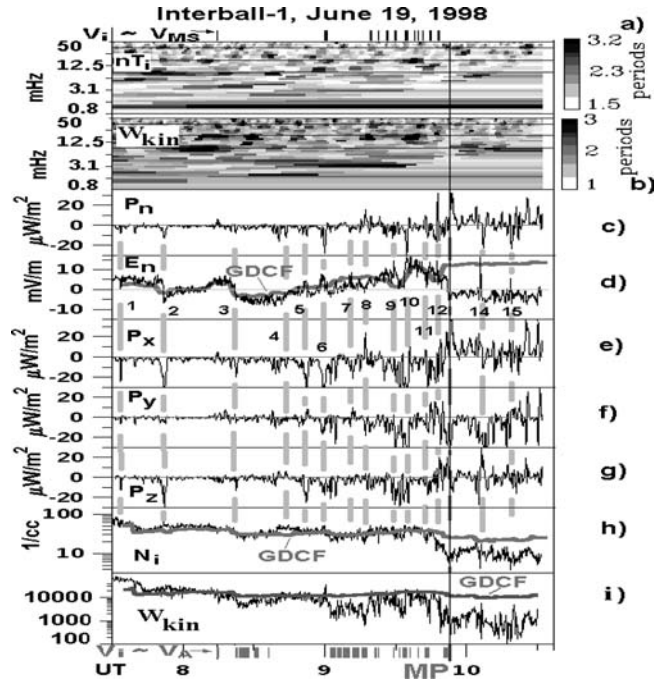


Figure 4. Tracing of disturbances in TBL on 19 June 1998; black vertical line – approximate MP crossing. (a) and (b) wavelet correlation time for ion thermal and kinetic energy densities, left – octave frequency scale in mHz, right – gray scale in periods of coherent signal at every frequency, black horizontal lines – 1st, 2nd and 4th spacecraft spin harmonics; (c) Poynting flux along MP normal (P_n , see Figure 2.A6 and related discussions) for 2–50 mHz; (d) electric field along MP normal and its GDCF prediction (thick gray line), the time lag at 08:30–10:30 UT is the same as in Figure 2.A6, the lag at 07:30–08:30 UT is 7.5 min less (numbers mark events discussed in the text); (e–g) Poynting flux along GSE X , Y and Z for 2–50 mHz; (h) ion density and its GDCF prediction (thick gray line). Top – black bars mark flows with \sim magnetosonic speed V_{MS} , bottom – gray bars mark flows with \sim Alfvén speed V_A .

direction. The GDCF proxy for E_n is represented by the red color, and shifted by an extra 1 mV/m for better adjustment with the experimental data. In panel c the magnetic field clock angle is presented in degrees: the black line is for the Interball-1 data, and the violet line shows SW monitoring by Geotail shifted in time to adjust to the average Interball-1 data at 09:30–10:00 UT. Predictions of GDCF at the Interball location are represented by the red line.

All three curves correlate at \sim 08:40–09:50 UT, proving an MSH encounter. Panel d of Figure 2.A6 displays $|B|$ in the same format (scale for SW in nT on the right side).

Systematic discrepancies between the data and SW proxy, which we call ‘plasma balls’, are shaded blue (cf. Figure 3). Note that at \sim 09:33 UT a similar field depression at Interball is predicted by GDCF. Only the appli-

cation of the model can provide a reliable tool to determine this crossing of the low-shear MP (at $\sim 09:53$ UT), which is imbedded in the TBL. The change of the sign of the ion velocity (\pm signs are marked by green/blue) in panel e (V_{ix} , GDCF – red line, scale in km/s) confirms the identification of the MP encounter. In panel f, the ion temperature T_i slightly reduces prior to the MP and then rises by a factor of 1.5–2. This reduction reflects a diminishing effective temperature of the core MSH ions as the T_i is fitted to the 3D Maxwellian ion distribution. The T_i does not account correctly for the input from higher-energy protons, clearly seen in panel h from 08:53 UT on. A similar remark is also applicable for the absolute value of nT_i in panel a.

In panels g and h of Figure 2.A6, electron and ion color-coded (scales for counts per second on the left side) energy spectrograms are presented, with the energy-per-charge scales in eV depicted on the left. Black lines give count rates of the ions and electrons with energies > 30 keV, which flow generally towards the Sun (count rate scales on the right vertical axes). Panel j of Figure 2.A6 depicts a wavelet spectrogram of the ion kinetic energy density, and panel k that of the thermal ion energy (vertical frequency scales are octave-based, i.e. logarithmic, cf. Figure 2.A5 and Figure 2.A6i). In panels l–n we present color-coded (see the logarithmic scale on the left side in $\text{cm}^{-2} \text{keV}^{-1} \text{ster}^{-1} \text{s}^{-1}$) spectrograms of energetic ions flowing towards the Sun (FOV 180° from the Sun, cf. black line in panel h), from the Sun (rotating FOV at 62° from the spacecraft spin axis, pointed to the Sun) and sunward flowing electrons (panel n, FOV 180° , cf. black line in panel g).

Returning to a comparison of the B_y -spectra from Geotail and Interball-1 (Figure 2.A5, 2.A6i), the time lag between Geotail and Interball-1 should be 5–15 min (Savin et al., 2002a). Within those lags a SW disturbance at $\sim 07:52$ UT on Interball-1 is quite similar to that at Geotail. In the middle of the MSH at $\sim 08:30$ UT another disturbance practically coincides with that of the SW, with the low-frequency part being strengthened in the MSH. At 09:00–10:50 UT in the MP vicinity, wide-band Interball-1 fluctuations are seen; most of them have no counterparts in the SW, and vice-versa. This implies that driving by the SW is not dominant for the near-MP period analyzed; note multiple spectral maxima in this region (TBL, see Figure 3), which are related in a complicated manner. At frequencies > 0.7 mHz the disturbances in the TBL have higher intensity levels and different frequency dependencies, as compared with the MSH; therefore we think that the MSH is also not the major source for the fluctuations in the TBL.

This is in agreement with the cross-correlation of B_y at 07:30–10:10 UT being < 0.5 ; at 09:30–10 UT the cross-correlation is 0.23, with a time lag for Geotail of 12 min, with Geotail $V_x = -478$ km/s. Considering possible different tilts for SW disturbances (Maynard, 2003) would hardly improve the correlation substantially. Greater resolution of these variations is presented in Figure 4, which will be discussed in detail in Section 2. After implementing

different lags in Figure 4d, we can see that in events 2, 3 and 10 the GDCF (i.e. SW) disturbances produce clear responses in the Interball data, while the TBL perturbations of a comparable magnitude in events 5–7, 9 and 11 have no counterparts in the SW (cf. also Figure 2.A6, panel c). Strong differences in the magnetic spectral shapes in the Interball-1 and Geotail data are also in agreement with the local nature of the TBL turbulence (Savin et al., 2002a).

Just inside the MP, energetic electrons have a high count rate (Figure 2.A6, panel g) that marks the boundary of closed magnetospheric field lines. This provides extra support for locating the PB inside the MP. Waves in the 2–50 mHz range (panels i–k) correlate with the intensity of energetic protons (black line in panel h and panels l, m) upstream of the MP, starting from ~08:53 UT. The main wave bursts have counterparts in the energetic electrons (panel g). The low-shear MP (~80°) and PB encounters take place at a tilt ~-21° (i.e. the Southern dipole axis being turned from the Sun towards the tail). The IMF B_z turned to positive values about 10 min prior to the MP. The ion plasma beta at 09:56–10:03 UT reached 15; in the rest of the blue-shaded sites it exceeds 2. Similar PB encounters occur on one previous and two following Interball-1 orbits, on 15–27 June 1998 (Savin et al., 2005, submitted).

2.2. DIRECT INTERACTION OF THE MAGNETOSHEATH FLOW WITH A ‘PLASMA BALL’

After this discussion of the general TBL and MP features on 19 June 1998, we embark on a detailed investigation of the TBL properties. The main physical problem to address is how the practically demagnetized PB is interacting with the incident MSH flow in the collisionless plasma. Due to the high beta both in the MSH and the PB, the magnetic forces are small, and only local electric fields and waves can provide the MSH flow deflection and/or dissipation. The electric field E_n near the MP can be supported by a surface charge at the MP-related current sheet (s), and it can deflect the incident MSH plasma to flow along the MP, while it cannot stop the normal flow in the absence of wave-induced effective collisions. The ‘local’ E_n , should be seen as a regular difference between the measured and SW-induced field (i.e. GDCF one). The MP transition at ~09:53 UT is manifested in the different sign as compared with the GDCF one. Figure 2.A6b shows that the difference is mostly wave-like; the only systematic difference upstream of MP is visible at 09:48–09:53 UT. Such a negative E_n (relative to the GDCF one) might contribute to the flow turning, but it should accelerate the incident particles towards the MP (instead of stopping them) if the measured high-amplitude waves provide an effective perpendicular conductivity. Thus, the waves constitute the major means for the boundary and the MSH plasma interaction in the case under study.

In Figure 4a–b we display wavelet correlation times (see Savin, 2002b, 2003a, for details) for the thermal and kinetic ion energy densities, which indicate for how many periods (at each frequency) the signal is coherent. Usually a signal conserving coherence for more than 2 periods at several consecutive analysis intervals can be regarded as a regular or coherent one. Panels c, e–g display the Poynting vector normal to the MP and its GSE components in the frequency band 2–50 mHz. In Figure 2.A6, the latter serves to outline the weak sunward moving disturbances (i.e. with positive P_n). In panel d we present E_n with different time lags at 07:30–08:30 and 08:30–10:30 UT. In Figure 4 h and i, the measured and GDCF ion densities and ion kinetic energy density are depicted with the same time lags. Thick gray vertical lines with interruptions mark characteristic disturbances to be discussed; they are numbered in panels d and e. At 07:30–08:20 UT strong post-shock activity is well seen in Figure 2.A6, (cf. Savin et al., 2002b). Both the spectral and correlation time maximums at 1–2 mHz are recognizable throughout MSH (Figure 2.A6j and Figure 4a–b). Savin et al. (2002a, b) outlined similar maxima in magnetic spectra on Interball and Polar at these times, but they couldn't detect continuous or coherent signals.

We draw attention to events 2 and 3 (Figure 4), where the measured E_n on average reproduces that of the GDCE. Thus, these events represent SW disturbances moving in the downstream MSH far from the disturbed TBL. Accordingly, all Poynting flux components are negative in these events (cf. Figure 3 and Interball-1 GSM position in Figure 2.A6 at 09 UT). The same is, most probably, valid for events 1, 4 and for the low-frequency E_n trends between events 9–10 and 11–12. So, moderate SW disturbances provide a validation for our Poynting flux measurements in the MSH. At 08:35–08:53 UT a weak activity in panels i–k (Figure 2.A6) resembles that of Figure 2.A5 and thus is driven by the SW. The respective maximum at ~4–5 mHz in correlation time (Figure 4b) could be traced from the post-shock region at 07:50–08:50 UT. The region at 08:50–09:50 UT is characterized by strong disturbances, which are not SW-driven ones (cf. Figure 2.A5 and panels a–e and i–k in Figure 2.A6). Soft energetic ions are registered there (panels h, l, m, Figure 2.A6) that correlate with the strong energy fluctuations and with the drop in the MSH kinetic energy. The latter drop is well seen after 09 UT in Figure 2.A6a and Figure 4i as a systematic difference between the black and thick red traces. Figure 2.A6e also demonstrates the larger departure of V_{ix} from the model after that time. Figure 2.A6e also demonstrates the larger departure of V_{ix} from the model after that time.

We check the density correspondence to the model in Figure 4h; the average measured density follows the GDCF proxy rather well until the diffuse MP encounter, with two exceptions at ~07:50 and 08:45 UT. The first density departure can be affected by a partial shock crossing, while in the second one the ion momentum ($-nV_{ix}$) is close to the GDCF prediction, but

it departs from GDCF after 09 UT. The general agreement confirms the reliable n_i measurements and, thus, the local dramatic W_{kin} decrease (Figure 4i). Note that the average MSH flow is subsonic ($W_{\text{kin}} < nT_i$, see Figure 2.A5a) and super-Alfvenic ($W_{\text{kin}} > B^2/2\mu_0$). On the top of Figure 4, black bars mark flows with nearly the magnetosonic speed, V_{MS} ; on the bottom gray bars mark flows with nearly the Alfven speed, V_{MS} . This is also shown schematically by thin arrows in Figure 3. Besides the accelerated MS-jet at 09 UT, there are a number of smaller MS-jets in the upstream TBL.

The decrease in W_{kin} mentioned above after 09 UT corresponds to a decelerated Alfvenic flow. In the upstream TBL those flows are mixed with the MS-jets. In the MSH upstream of the TBL at 08:40–08:50 UT the standard deviations of ion energy densities are: $\delta W_{\text{kin}} \sim 22\%$, $\delta nT_i \sim 10\%$. Figure 2.A6k shows that at 08:53–09:35 UT nT_i fluctuates, at 09:03–09:15 UT the nT_i -disturbances dominate over those of W_{kin} : $\delta W_{\text{kin}} \sim 49\%$, $\delta nT_i \sim 20\%$, $\delta W_{\text{kin}}/\delta nT_i \sim 0.48$. In the middle of the upstream TBL both the kinetic and thermal ion energies are quite disturbed (09:15–09:35 UT): $\delta W_{\text{kin}} \sim 71\%$, $\delta nT_i \sim 25\%$, $\delta W_{\text{kin}}/\delta nT_i \sim 0.996$. Relative to the unperturbed MSH the standard deviations in the TBL center are: $\delta W_{\text{kin}} \sim 45\%$, $\delta nT_i \sim 17\%$. The lower limit for the energy conversion into the irregular fluctuations in the TBL (i.e. the difference of standard deviations) is 23% of MSH kinetic energy and 7% of its thermal. As the TBL spectra in Figure 2.A6j and k are quite different from the upstream MSH ones, we would like to accept the higher limits for the MSH energy chaotization: $\delta W_{\text{kin}} \sim 30\text{--}40\%$ and $\delta nT_i \sim 10\text{--}15\%$.

A strong deficit of the average W_{kin} at 09:03–09:15 UT (and of the ion momentum) is displayed even in the sum of $W_{\text{kin}} + \delta W_{\text{kin}}$, which constitutes only 47% of the average upstream kinetic energy. The only candidate to carry off the momentum and kinetic energy excess is the strong impulse in the W_{kin} and V_{ix} in Figure 2.A6 and Figure 4 at ~ 09 UT. The respective hodogram of the ion speed vector tip in the plane of GSE (V_x, V_y) is shown in Figure 5a. The average speed in the depicted interval 08:59:11–09:00:08 UT is $(-252, -45, -88)$ km/s, and the possible inferred vortex component (i.e. the loop in the hodogram) has a radius of ~ 50 km/s ($\sim 4\%$ of its average W_{kin}). Those estimates are given in the spacecraft frame (which is close to the MP frame), while in the frame of the unperturbed MSH the vortex kinetic energy is $\sim 0.3 W_{\text{kin}}$. Since the magnitude of the W_{kin} -pulse reaches the local value of nT_i (Figure 2.A6a), that means a nearly magnetosonic (MS) speed of the jet ($V_{\text{MS}} \sim (2T_i/M_i)^{1/2}$ in the high-beta plasma (M_i – proton mass, T_i – in energy units)). A magnetic loop at this time has been found at half this frequency.

This plasma jet is in the middle of a current sheet (bi-polar disturbance in the clock angle, Figure 2.A6c), bounded by $|B|$ drops down to a few nT ('diamagnetic bubbles') and a bi-polar E_n - spike (~ 5 mV/m), which can be

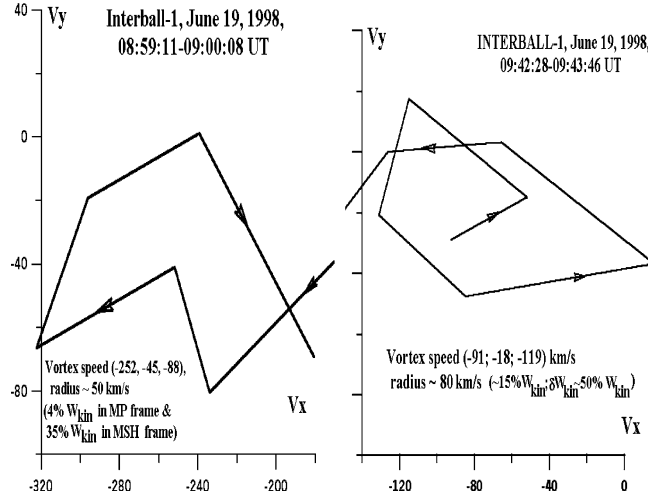


Figure 5. Left: Hodogram of ion V_x , V_y at 08:59:11–09:00:08 UT, 19 June 1998. Right: Hodogram of ion V_x , V_y 09:42:28–09:43:46 UT, 19 June 1998.

accounted by surface charges at the current sheet. In Figure 4 it is event 6 that contains the impulsive density rise. The negative spike of the Poynting flux in all components (for 5–50 mHz GSE vector being $(-20, -6, -5) \mu\text{W}/\text{m}^2$, i.e. at $\sim 24^\circ$ to the model speed $(-247, -6, -157) \text{ km/s}$, departing from the model flow towards the $-X$ and $-Y$ directions) in event 6 conforms to the energy being pushed downstream by this strong nonlinear structure. The value of $P_n \sim -10 \mu \text{ W}/\text{m}^2$ indicates the approach of the disturbance to the MP (see Figure 3). The latter excludes a near-MP reconnection as a mechanism for the jet acceleration: (a) any MP-related disturbance should move outward from the MP (i.e. $P_n > 0$); (b) the distance from the MP is too large (in ~ 1 h prior to its crossing); the GDCF does not predict any substantial outward MP movement in this period; and (c) negligible $|B|$ just inside the MP and in its vicinity (the magnetic energy density is about an order of magnitude less than that of the W_{kin} spike in event 6) can hardly result in such a strong plasma flow acceleration of up to an Alfvénic Mach number ~ 3.1 in the MS-Jet.

Between the event 4 and the MP we can see strong enhancement in the appearance of the negative (downstream) P_x , P_y and P_z -spikes (events 5–7 and 9), which correspond to local TBL disturbances without correlative feature in SW (cf. Figure 2.A5 and 2.A6). Similar to event 6, the events 5, 7, 9 have related clock angles and electric field spikes, while the plasma jetting is unique for event 6.

There is another group of perturbations with positive P_n -spikes, i.e. moving from the MP towards the outer TBL border that are numbered 8, 10–12 and MP (see also Figure 2.A6b). The P_n -positive events dominate

there, and event 12 has positive P_y and P_z moving upstream along the MP. The MP-related perturbation moves in the positive X and Z directions but strongly in the negative Y direction. Event 14 inside the MP resembles a short double MP crossing, but generally moves from the MP (negative P_n), as does event 15. Between events 6 and 7 weak positive P_n -spikes of short duration can be seen.

The ion velocity hodogram in the GSE plane (V_x , V_y) for the trailing part of event 11 with negative components of the Poynting vector is depicted in Figure 5b. The average speed in the interval 09:42:28–09:43:46 UT is (−91, −18, −119) km/s, and the inferred vortex component has a radius of ~80 km/s (i.e. 15% of its average W_{kin}). Thus, the vortex energy is big enough for a non-linear wave, since it contains >33% of the chaotic kinetic energy. No obvious vortex-like magnetic loops have been detected around event 11. Correlation times in Figure 4 provide information on the coherence of the disturbances. W_{kin} ‘synchronization’ at ~5 mHz (09:15–09:45 UT) corresponds to the appearance of the positive P_n – spikes in the TBL center. The reflected (sunward going) wave packets provoke interactions in the upstream region closest to the MP. At 08:45–09:35 UT (events 4–10) the strong maximum at ~3 mHz in the W_{kin} correlation time most probably results from regular launching of tailward wave packets from the outer TBL boundary. The maximum at 3 mHz is also seen in Figure 4a. Inside the MP the quasi-coherent signals are at ~7 mHz, and that corresponds to Pc4 pulsations.

To give more details for the TBL interactions upstream of the MP, we zoom in on the interval 08:30–10:00 UT in Figure 6.B1 and 6.B2, showing wavelet spectrograms for the ion density and velocity V_{ix} , respectively. The former is similar in its main features to the panel k in Figure 2.A6. The latter is quite compatible with panel j in Figure 2.A6 and provides the direct comparison with a bi-spectrum in Figure 6.B3. Figure 6.B1 demonstrates the strengthening of the low-frequency (~1.3 mHz) maximum just upstream of the plasma jet for event 6 (09 UT). The coherent signal at 4–5 mHz (panels a, b, Figure 4) can be related with a weak maximum at ~4.2 mHz. Referring to the Poynting flux in Figure 2.A6 and Figure 4, we conclude that the weak waves at ~4.2 mHz propagated upstream and triggered amplification of the down-going low-frequency waves. The weak maximum at 4.2 mHz is visible at 08:48–08:55 UT in Figure 6.B2 along with the stronger one with a rising tone from ~1.5 to 2 mHz. The latter grows further in magnitude and frequency (~2.3 mHz) until 09 UT (event 6, i.e. launching of the plasma jet), where it bifurcates into rising- and falling-frequency tones, which evolve toward about 1.3 and 2.7–3.5 mHz bands (cf. correlation time maxima in panels a, b in Figure 4). At ~09 UT maxima at about 5 and 12 mHz are also visible. In the upstream TBL at 09:00–09:45 UT the kinetic energy drops mentioned above result not only in plasma jetting but also in amplification of

the low-frequency pulsations (~ 1.3 mHz), three periods (~ 10 – 15 min) of which cover almost the whole upstream TBL. Those fluctuations correspond to maximums at 3–10 mHz at $\sim 09:00$, $09:15$, $09:30$ and $09:45$ UT. A macro-equilibrium can be achieved in the outer BL (Figure 3) during a few of these periods. This is in agreement with a ‘thick’ TBL transition invoked by Savin et al. (2001) versus a ‘thin’ shock-like one.

To check if the nonlinear processes in the outer TBL are really synchronized, we analyze the wavelet bi-spectrum (bicoherence) for the velocity V_{ix} in Figure 6.B3, which corresponds to a frequency sum rule for the 3-wave process, $f_s = f_l + f_k$. The bicoherence has a substantial value only if those three processes are phase-coupled (cf. Savin et al., 2002b); the modulus of the product of the 3 complex wavelet amplitudes is normalized by the modulus of the amplitude of the three signals at their respective frequencies. This corresponds to decays (or a junction), which require a third-order non-linearity in the system. The weaker, higher-order nonlinear effects, which might also contribute to the TBL physics, are beyond the scope of this paper. In Figure 6.B3 we display the bicoherence of V_{ix} at $08:42:57$ – $09:12:51$ UT for $f_k \sim 1.5$ – 8.5 mHz (the larger frequency in the sum) and $f_l \sim 1.5$ – 5 mHz. The horizontal and vertical lines indicate processes with nearly constant f_l and f_k , respectively, and the negatively inclined line marks processes with $f_s = f_l + f_k \sim \text{constant}$. We show only processes with the relative amplitude > 0.5 (50% of the triple product absolute value), i.e. all colors, except the dark blue background, mark signals whose bicoherence is certainly above the noise level (cf. maximum bi-spectral amplitudes are $\sim 50\%$ in Savin et al. 2001, 2002b, 2004).

Neglecting the frequency drifts near the bifurcation point at 09 UT in Figure 6B.2, we can distill the processes in Figure 6.B3 at several frequencies: $f_l \sim 1.5$ mHz, lower horizontal maximum, cf. ~ 1.3 mHz in Figure 6.B2 and in Figure 4; $f_l \sim 2.2$ mHz, upper weak horizontal maximum, compatible with the general upstream maximum at $08:50$ – $09:00$ UT in Figure 6.B2; $f_s = f_l + f_k \sim 4.5$ mHz (the lower inclined line), which is close to the upper downstream maxima at $09:10$ – $09:40$ UT in Figure 6.B2 and to that of upstream maxima in Figure 6.B1, 6.B2 and Figure 4; $f_k \sim 2.2$ – 2.6 mHz, strong vertical maximum (cf. panel b in Figure 4 and Figure 6.B1, 6.B2) with the largest amplitude at its top. The latter red spot corresponds to the second harmonic generation: (cf. Savin et al., 2002b), visible at 09 UT at ~ 5 mHz in Figure 6.B2 (MS-jet). Another red-spot maximum would suggest wave pumping at $(f_l, f_k) \sim (1.5, 3)$ mHz with further nonlinear cascading at $f_s = f_l + f_k \sim 4.5$ mHz (lower inclined line) and at $f_l \sim 1.5$ mHz (see the lowest horizontal maximum up to 6 mHz (Savin et al., 2001, 2002b)). We assume that the cascade signatures (e.g., in the case of the horizontal-spread maximum, when at the sum frequency, $f = f_1 + f_2$, the bicoherence has a comparable value with that at the starting point (f_1, f_2)), implies that the wave

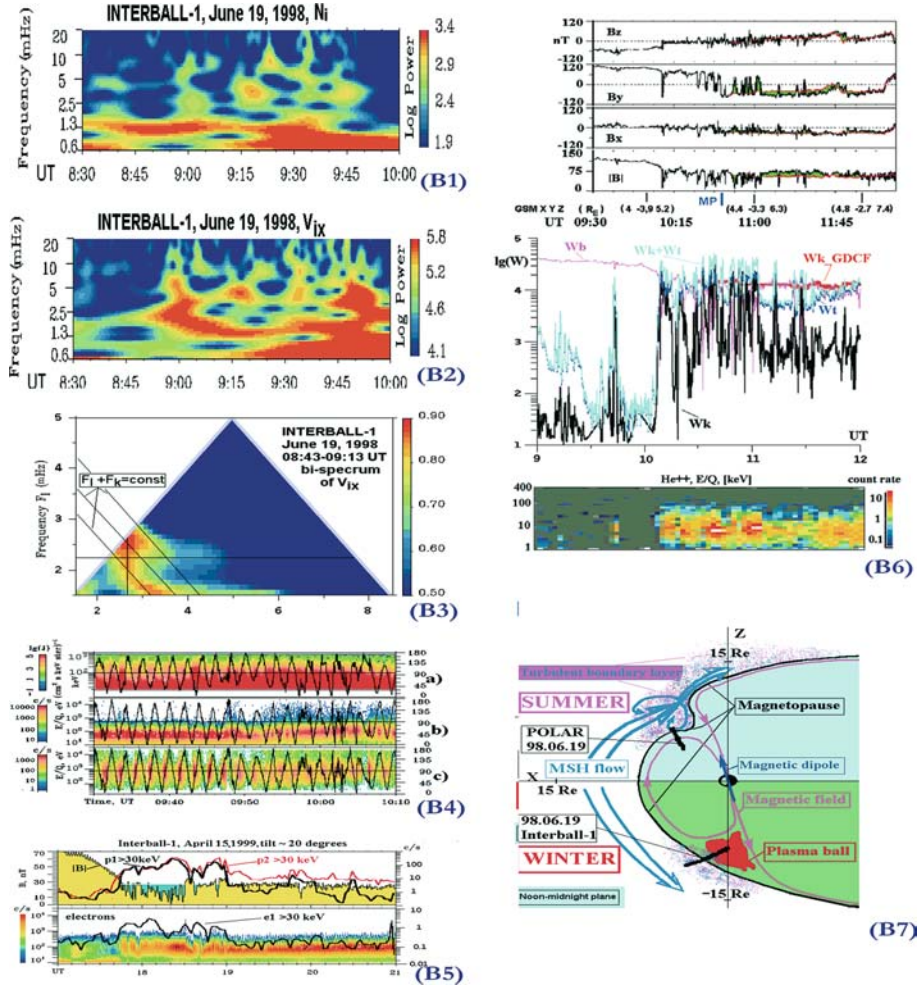


Figure 6. (B1) Spectrogram of ion density, 19 June 1998. (B2) Spectrogram of velocity V_{ix} , 19 June 1998. (B3) Bi-spectrum of velocity V_{ix} , 08:43–09:13 UT. (B4) Ion (a, c) and electron (b) spectrograms and pitch-angles (right scale), Interball-1, 09:30–10:10 UT, 19 June 1998. B5: Open OT, 15 April 1999. Top: $|B|$ (yellow-marked) and protons (> 30 keV, p2 (red)- from Sun, p1- towards Sun). Bottom: electron spectrogram and intensity (> 30 keV, towards Sun). (B6) TBL crossing by Polar, 19 June 1998. Top: GSM magnetic field versus GDCF (red line). Middle: Magnetic (violet line), thermal (blue) and ion kinetic (GDCF – red line) energy densities and their sum (light blue). Bottom: He^{++} spectrogram. (B7) Sketch for MSH interaction with cusps.

at the sum frequency interacts in turn with the same initial wave at frequency f_1 in the following 3-wave process: $f_3 = f_1 + f$, etc. Note also horizontal and vertical cascading at the frequencies of 2.2 and 2.6 mHz mentioned above. The linkage between the spectrogram maxima represents a feature of cascade-like processes in Figures 2.A6, 6.B1 and 6.B2. Thus the bi-spectrum

provides strong support for the decay-like phase coupling of the low-frequency fluctuations in the upstream TBL.

We have also checked the wavelet spectra and bi-spectra for ion density, kinetic and thermal energies and observed a highlighting of similar processes up to about 20 Hz. The 3-wave nonlinear wave-coupling persists also in the TBL central and inner zones (not shown). Similar to the magnetic spectra in Figure 2.A6, the simultaneous magnetic bi-spectra (not shown) differ in detail from those of Figure 6.B3. First of all, the magnetic bi-spectra have lower maximum magnitudes (up to 0.6 instead of 0.9 in Figure 6.B3). Thus, in the high-beta plasma the energy-dominated ion moments are the most representative ones for understanding the nonlinear interactions.

2.3. COMPARISON WITH POLAR DATA ON 19 JUNE 1998

Let us briefly compare the Interball-1 data on 19 June 1998 with the simultaneous Polar data in the northern hemisphere (tilt $\sim 20^\circ$). Referring for details to Dubinin et al. (2002), Savin et al. (2002a, b), we present the Polar outbound crossing in Figure 6.B6. The magnetic field at the top of Figure 6.B6 highlights the MSH encounter in B_y , changing from positive magnetospheric values to negative MSH ones, which conforms to the GDCF predictions (shown by the red line; the difference from the measured field is highlighted by the green color). We mark MP (separating average MSH and magnetospheric fields) for traverses of the magnetopause current sheet, which may be multiple. Note that the MP is at GSM $Z \sim 6 R_E$ versus $-10 R_E$ for Interball-1. The respective orbit traces are given by thick black lines in Figure 6.B7. In the middle panel of Figure 6.B6, we display energy densities similar to Figure 2.A6. The spiky bursts of the kinetic energy density (black line) have been attributed by Dubinin et al. (2002) and Savin et al., (2002a, 2002b) to reconnection bulges. We can see from a comparison with the model kinetic energy and between the measured and model magnetic fields that the bulges' appearance is controlled mostly by the local TBL processes (i.e. no SW driving is proved by GDCF). The micro-reconnection in the bulges should be modulated by the upstream TBL fluctuations (see previous Section), since the spectral features of the magnetic fluctuations (in the band of the repeated reconnection bursts) in the transition region at 10–11 UT are quite similar to those measured by Interball-1 in the upstream TBL (see Savin et al., 2002a). So, the current sheets at $\sim 10:50$ – $11:05$ UT are attributed to the TBL.

Another point that we would like to make is that the kinetic energy in the 'reconnection bulges' at 10–11:20 UT exceeds the GDCF model predictions (red thick line on the middle panel) by 1.5–2 times. Even inside the MP the magnetic field energy density has a smaller magnitude than that of ion total

energy (light blue curve) in the jets. We compare the magnetic field energy with the total ion energy because, with reconnection, the transformation of stored magnetic energy from the MSH flow to magnetosphere should go in kinetic and then partially into thermal ion energy of the bulge-related streams of the plasma. The accelerated jet at the outer TBL border (see event 6 in Figure 4 and Figure 2.A6) has similar characteristics to the spiky bursts in Figure 6.B6, which makes it a good candidate source for the regular plasma jets registered by Polar (Figure 6.6).

2.4. ACCELERATED PARTICLES

Recent multi-satellite observations demonstrate that the cusp is a region of accelerated plasma. There is evidence that the cusp is a substantial source of energetic particles (Q. Chen et al., 1997, Fritz et al., 2000). The energization mechanism is related to the strong turbulence observed in the cusp (Chen and Fritz, 1997, Blecki et al., 1998, Savin et al., 2002c), and recently mapped by Interball-1 (see Section 3). Ions with energies over 7 keV on 19 June 1998 are seen after 08:50 UT on the spectrograms in Figure 2.A6h. As mentioned above, waves in 2–50 mHz range (panels i–k, Figure 2.A6) correlate with the intensity of energetic protons upstream of MP.

Turning now to the spectrograms in panels 1–m (Figure 2.A6), we see that the upstream ions correlate best with the W_{kin} -fluctuations (panel j), the yellow-colored fluxes at high energies at 09:20–09:50 UT exceed those of the trapped particles inside the MP. The maximum intensity of the energetic ions occurred just inside the MP (i.e. in the PB) with the ion intensity decreasing farther inside the magnetosphere (better seen in panel m). The higher energy ions, correlating with the upstream TBL fluctuations, suggest local acceleration. The electron spectra in panel n of Figure 2.A6 upstream of the MP also generally correspond to the intensification of fluctuations in W_{kin} , with electrons up to 50 keV appearing. In Figure 6.B4 we zoom in the electron and ion energy spectrograms from Figure 2.B6 at 09:30–10:10 UT, adding respective pitch-angles (scales in degrees on the right side). Before 09:47 UT (i.e. in the MSH) electrons (panel b) and ions at 7–25 keV (panel c) tend to have a minimum flux in the field-aligned direction. This excludes reconnection as a source for the higher energy ions, as in the southern hemisphere the magnetospheric field is pointed away from the Earth, thus particles, escaping from magnetosphere, should flow parallel to the reconnected lines (cf. Savin et al., 1998b, 2004). The only higher energy electron burst, at 09:48 UT, also demonstrates a domination of the anti-parallel flow. The main MSH ion maximum upstream of the MP occurs at pitch angles $\sim 90^\circ$ and spreads up to 25 keV (panel c), and this

strongly infers a local source for the most dense suprathermal ions. At 09:55–10:05 UT the ions at 7–25 keV are peaked at $\sim 90^\circ$ along with the most MSH-like ones. Their fluxes along the field are smaller than the perpendicular fluxes, but they exceed the anti-parallel fluxes. The latter might imply either a minor amount of the plasma-sheet-like (PS, energies 7–25 keV) ions along the field lines from the inner magnetosphere or represent a loss-cone towards the nearest (southern) ionosphere.

In Figure 6.B4a we zoom in on panel m of Figure 2.A6 and superimpose the respective pitch angle. Around 09:40 UT soft ions with energies < 50 keV display a minimum along the magnetic field, similar to that in panel c. This gives an estimate for the upper limit of supra-thermal ions of MSH origin. At higher energy (up to 400 keV) the parallel ion flows dominate, and this conforms to their leaking from the PB along effectively reconnected field lines. Further support for that can be found in bottom panel of Figure 7; both the intensity and slope of the average ion energy spectra at energies > 200 keV almost coincide for the PB (curve 3) and TBL (curve 2). An instant spectrum of the field-aligned ions in the TBL (i.e. leaking along the field line from PB, shown in curve b) from the time interval 09:40:37–09:42:02 UT reproduces the average shape of the PB spectrum (curve 3), but with a slightly smaller intensity.

Coming back to panel a in Figure 6.B4, around 09:40 UT there are also narrow perpendicular spikes at the higher energy levels, which constitute the third population of energetic particles in the upstream TBL. Having practically no parallel speed, these ions can result, for example, from local perpendicular ion-cyclotron acceleration. To justify an alternative magnetospheric origin of those ions we should explain their loss of parallel energy; such ions are not seen in the OC, and to be able to reach the outer BL from distant regions along the MP they should have a parallel velocity comparable with their perpendicular velocity. In Figure 7 the respective characteristic energy spectra are marked by ‘a’ and ‘b’ in the top panel and by ‘a’ in the bottom panel. A difference between the maximum spectra (‘a’) and that of the PB spectra (curve 3) is highlighted by shading, and reaches a factor 3. The spectral shape is representative on the top panel (this channel does not rotate and has nearly constant pitch angle during the exposition of spectrum ‘a’). Comparison with panel a in Figure 6.B4 suggests that the highlighted spectral difference is a systematic one. Even the average spectrum in the TBL (‘2’, top panel in Figure 7) is slightly larger than that of the PB at energies > 250 keV. Panel a in Figure 6.B4 in PB at 09:53–10:05 UT demonstrates loss-cones in the anti-parallel magnetic field direction (cf. panel c). The energetic particle culminating in the PB just under the MP can result both from the local cascading of chaotic kinetic energy and from loss of parallel momentum by magnetospherically trapped particles undergoing a wave-particle interaction. This is also necessary to trap the locally-born accelerated

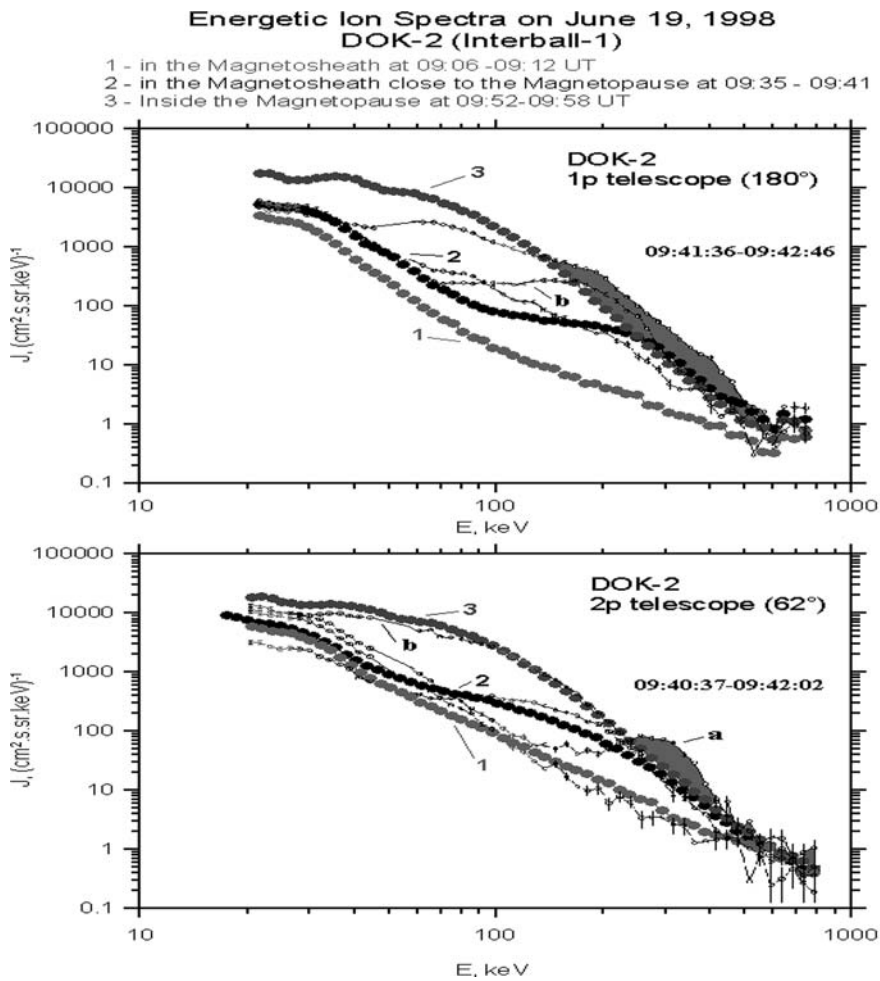


Figure 7. Energy spectra on 19 June 1998 for sunward (top, FOV 180° from Sun) and tailward (bottom, FOV 62° from Sun) flowing energetic ions; thick circles: 1 – MSH 09:06–09:12 UT, 2 – TBL 09:35–09:41 UT, 3 – PB 09:52–09:58 UT. Small thin circles: top – 09:41:36–09:42:46 UT, bottom – 09:40:37–09:42:02 UT. Shading marks the difference between PB ('3') and TBL perpendicular spectra denoted by 'a'.

particles in the PB, for example, the soft energetic ions < 150 keV (curves labeled '3' in Figure 7) can leak from the magnetosphere (curve 'b' on bottom panel) due to diffusion by the strong waves (cf. Savin et al., 1998b, 2002c).

On the bottom panel in Figure 6.B6 we present a color-coded (see color bar for the logarithmic count rate on right side) spectrogram of energy per charge (logarithmic scale in keV/e is shown on the left vertical axis) for the unique MSH constituent He^{++} . This clearly demonstrates the local acceleration of He^{++} up to 100 keV/e in the region of numerous plasma jets and

MP-like transitions at 10–11 UT (see the upper panels and discussion above). Another peculiarity is a much greater intensity as compared with the MSH stagnation region after 11:30 UT.

As for more energetic particles (not shown), the acceleration of ions up to several hundreds of keV and of electrons up to several tens of keV is seen in the TBL, with a maximum at the multiple B_y transitions (10:20–11:10 UT). Note also the difference with the Interball data: no enhanced energetic particle fluxes inside MP are registered by Polar. A similar case in the OT on 21 April 1996 from Interball-1 data has been described by Savin et al. (2002c). The electrons with energies up to 10 keV can be accelerated by whistler-mode fluctuations of about 1 Hz (see Savin et al., 1998b). Another case of the OT is presented in Figure 6.B5. Top panel depicts $|B|$ (yellow shaded, scale in nT on left axis) and energetic ions (>30 keV, logarithmic scale for counts/s on right side) from the same channels as shown in panels 1–m in Figure 2.A6 (the 180° channel is marked by a black line) during an outbound MP crossing on 15 April 1999 (at $\sim 17:45$ UT). The large-scale $|B|$ reduction is shaded green, and looks similar to the PB in Figure 2.A6, but in this case the energetic ion intensities comply with the particle source being the MSH rather than the magnetosphere. The anti-sunward flowing ions (red line) have a greater flux in the MSH than inside the MP and dominate the sunward flux. Therefore, similar to Figure 6.B6, we attribute the magnetic field reduction at tilt $\sim 20^\circ$ to the OT. Both energetic ions and electrons (bottom panel) have strong clear maxima in the OT and just upstream of it, which represent a feature of local particle origin and/or accumulation.

3. Turbulent boundary layer encounters by Interball-1 (1995–2000)

To complement the TBL encounters on 19 June 1998, we present a survey of encounters with the TBL by Interball-1 made during 1995–2000. The Interball-1 orbit evolution provided an opportunity to cross the near-cusp MP along with the boundary between the mantle and LLBL in the near tail twice per orbit (excluding the late October – late December period). For this study we use the routinely calculated dispersion of the B_x raw magnetic field waveform with a sampling rate of 4 Hz over 2-min intervals (i.e. for 0.0085–2 Hz). We multiply the B_x dispersion by a factor of 3 for comparison with Df in a statistical sense (i.e. we suggest equality of the ULF average power for all 3 magnetic components). We give the AC magnetic pressure (Df) in eV/cc for comparison with the other energy densities. Similar to Savin et al. (2002a), we define the background TBL when in a time interval of < 20 min the B_x -variation during 2-min intervals exceeds, at least at two points, the threshold $3 nT$ ($\sim 5.2 nT$ for full variation or ~ 67 eV/cc). This is 1.5 times higher than that of the nearby MSH. This is shown by gray-colored orbit

pieces in Figures 2.A1, 2.A2 and 2.A4. Note that in previous TBL statistical studies (Savin et al., 1999, 2002a, 2003a) a shorter time period of 1–3 years and a variation interval of 20 s have been used.

We have checked for several characteristic TBL cases that the 2-min variation interval is rather representative as Df starts to saturate with an increase of the variation interval. We have found 651 TBL events on about 400 MP crossings; thus, most MP crossings have multiple TBL encounters according to the above definition. In Figure 2.A1 we display in 3 GSM planes the color-coded distribution of the events with high magnetic variance, as function of the B_x -variation magnitude ($D(B_x)$), with the colors for the respective variation intervals depicted in the left lower corner. We limit our study to the region outside the magnetosphere by requiring that one of the minimum of two values is satisfied: (a) half the distance between the point most distant from the Earth’s MP and the point closest to the Earth’s bow shock (BS) in the same orbit, and (b) $5 R_E$ beyond the most distant MP. We exclude single spikes in the B_x -variation, which clearly correspond to the main magnetic field changes at the MP itself. The gray-colored TBL background serves mostly to mark the near-MP coverage by the Interball-1 orbits. Note the data gap for $Z < -14 R_E$ and $|X|, |Y| < 7 R_E$ (which is due to the Interball-1 re-entry in October 2000). The tail MP around midnight is not covered by Interball-1 (the shaded data gap area in the center of XY -plane), while the dayside one is.

In Figure 2.A1 all events concentrate at high latitudes ($|Z| > 4 R_E$) near the OT and downstream from it, and are especially well seen for variations $> 8nT$ (blue and red colors). Those events are associated with the TBL per se. In the YZ -plane at low latitudes we can also recognize groups of intensive events (for both positive and negative Y), while the projection XZ -plane demonstrates that most of them are encountered in the tail. The latter corresponds to the ‘sash’ of a prediction (Maynard et al., 2001). The northern (upper) TBL is indented in the YZ -plane, corresponding to the MT indentation (cf. Savin et al., 1998a, b and Figure 1). In the southern hemisphere no indentation can be inferred. To prove that this is not an effect of an absence of coverage at large negative Z , we compare the appearance of events along directions $Z = 10 R_E$ and $Z = -10 R_E$: in the former case there is a clear maximum in the vicinity of $Y \sim 0$, while in the latter case there is a minimum in the event occurrence (shifted to positive Y). The peculiarities mentioned above are even better seen in Figure 2.A2, where the gray-scaled background events are given in the same format, while the rest of the color-coded ones are shown only for B_x -variations $> 8nT$ (see the discussion of tilt dependence below). In Figures 2.A1 and 2.A2 we mention the TBL ‘wings’ in the XY and XZ planes, ranging from the near-cusp TBL into the tail down to $X \sim -20 R_E$. The higher-latitude ‘wings’ are in the vicinity of the boundary between semi-open mantle lines and closed LLBL lines. The local minimum in the total

magnetic field and the associated currents, which provide the field rotation from the open to closed lines are anticipated there. In the TBL, compressional magnetic field disturbances are also present.

While they are not dominant in the TBL power, the spiky magnetic field decreases, ‘diamagnetic bubbles’ (DB, see Savin et al., 1998b) provide a mechanism for plasma heating in the TBL. It has been demonstrated in a number of case studies (see Savin et al., 2004, and, references therein) that the DB differ from mirror waves by an absence of perpendicular ion energy dominance. For the DB statistics Savin et al. (1999) used the maximum depths of the spiky total field ($|B|$) drops to calculate the diamagnetic effect of the heated MSH plasma inside the DB. The DB distribution (not shown, but see, e.g., Romanov et al., 1999) is generally the same as the TBL events shown in Figures 2.A1 and 2.A2. The averaged maximum plasma pressure excess in the DB is $\delta(nT) = 2160$ eV/cc. The magnetic field inside the ‘bubble’ is about 8.3 times weaker than outside. Taking the plasma density in the TBL to be 5–10/cc, we observe plasma heating to 216–430 eV inside the DB, i.e. heating of 1.5–3 times the temperature of the MSH ions. This is in good correspondence with the predictions of Haerendel (1978). Most events with $Df > (15nT)^2$ and $8(nT) > 3100$ eV/cc at $|Z| > 4 R_E$, with a prominent maximum above the cusp. Intensive heating in the high latitude tail ‘wings’ is seen only to $X = -6 R_E$.

Merka et al. (2000) concluded that the most prominent dependence of the cusp position is the dependence on dipole tilt angle. Their study was restricted to the northern hemisphere, where the tilt was positive for the majority of MP encounters by Interball-1/Magion-4. Their definition of the exterior cusp includes the TBL as a part. In Figure 2.A2 we present a map of TBL events, color-coded by the magnetic dipole tilt angle (see the colors and corresponding tilt ranges in the bottom left corner). For the analysis we have chosen only strong TBL-like events with the B_x -variation $> 8nT$ (480 eV/cc). In the northern indentation, the events with positive and zero tilts dominate for $Z < 10 R_E$. This agrees with the direct interactions of the open cusp throat with the incident MSH flows (marked “1” in Figure 1). The indentation in the TBL/MP does not represent a characteristic feature of the winter hemisphere; the events with negative tilts strongly dominate near $Y \sim 0$ at negative Z in the YZ -plane. This asymmetry suggests that the interaction of the MSH flow can be different for negative and positive tilts.

4. Statistics for plasma balls and open cusp throats

We now return to the largest scale nonlinear sites in the outer cusp, which we call ‘plasma balls’. Figures 2.A6 and 6.B6 demonstrate that at sunward and anti-sunward tilts (i.e. from Polar and Interball-1 data) the MSH flow

interaction includes similar features, e.g., accelerated plasma jets and stagnant heated MSH plasma at the MSH-cusp transition. The general difference is that for positive (sunward) tilts this stagnant plasma is located outside the MP (as Figure 1 and Figure 6.B6 infer), while the PB in Figure 3 and Figure 2.A6 is certainly inside it (see also Savin et al., 2002a). This means that the cusp throat can be open for direct interaction with MSH flows (OT) or closed by the MP, depending (presumably) on the tilt sign. Thus, streamlines of the MSH flow around the cusps can be asymmetric, as shown in Figure 6.B7 (where Interball-1 and Polar traces from Figures 2.A6 and 6.B6 are marked by thick black lines).

In the summer (positive tilt) hemisphere, the MSH TBL is located in the MP indentation over the cusp. In the winter (bottom), the TBL is located both upstream of the MP and at the outer PB border; while the MP indentation might exist it is not so deep as the summer one (cf. Figure 2.A1, A2). We use the same full Interball-1 database shown in Figure 2.A1, A2 to explore how characteristic such occurrences of PB are. In most high-shear cases and when energetic particles mark a clear trapped boundary, as in Figure 2.A6, we recognize the PB from key parameters and from energy-time spectrograms of the thermal particles, using the characteristic features discussed above.

For ~30% of more complicated cases (from 52 PB in Figure 2.A3, A4 and from 37 magnetic field cavities with heated plasma in the open OT in Figure 2.A4) we have analyzed the pitch-angle distributions (cf. Figure 6.B4) or detailed IMF data. We have set the lower duration limit for the large-scale PB at 10 min, the smaller ‘diamagnetic bubbles’ have been studied earlier using only high-resolution magnetic field (Savin et al., 1998; Romanov et al., 1999, 2002a). In Figure 2.A3 we present the distribution of PB in three GSM projections. Gray-colored marks demonstrate rather dense Interball-1 coverage of the near-MP region (see Figure 2.A1, A2 and discussions above). Most of the PB are concentrated over the cusp throats at negative tilts (blue lines). They tend to occur at the outer TBL border (farther than $\sim 8 R_E$, and better seen in the northern hemisphere) and have maximum spread in the Y direction. Some of them are registered in the near tail, including most of those at positive tilts (red lines). The spread in the X direction is presumably due to different SW dynamic pressures; for example, the blue line at $X > 10 R_E$ closest to the Sun corresponds to the case on 11 May 1999, when the SW almost disappeared, and its size of $\sim 2.5 R_E$ provides a proxy for the upper PB size limit in the X direction.

A reasonable estimate for the average PB size from Figure 2.A3 would be $1\text{--}4 R_E$, and the Y -size could be over $5 R_E$. The PB width, inferred by Savin et al. (2002a) for 19 June 1998, is close to the upper limit. For 18–19 February 1997, with very stable SW conditions (Romanov et al., 1999), an estimate for the PB spread along the orbit from the satellite-subsatellite time lag is over 2

R_E . Taking into account an average MP speed of ~ 20 km/s (versus 1.5 km/s for the spacecraft speed), we can accept the average PB scale to be closer to the upper limit of its geometrical size in Figure 2.A3.

The PB has been identified as $|B|$ large-scale decreases with newly heated plasma inside the MP (Savin et al., 2002a). Before applying the GDCF, the PB had been thought to be located outside the MP similar to the stagnation region registered at the beginning of Interball-1 operation (Savin et al., 1998b). We have found 37 cases of the latter type, which resemble Figure 6.B5, having clear magnetic field, energetic particle behavior or particle pitch-angle features of the MSH (cf. Figure 6.B4 at $\sim 09:40$ UT). The general difference of these cases from those of the PB is that the MP, while being embedded into strong perturbations, effectively isolates the MSH electrons and most of the ions from the magnetosphere.

Another difference is that at the PB outer border the fluctuations, generated in the process of the MSH kinetic energy dissipation (see Figure 2.A6 and respective discussion above), are combined with dissipation at the MP *per se* (separated in the case of OT). This enlarges the fluctuation level and, consequently, enforces turbulent transport processes. The tilt dependence of the occurrence of PB and OT is presented in Figure 2.A4. Blue bars mark the number of PB in a dipole tilt interval, while the red bars mark the stagnant MSH outside the MP – the OT having large-scale $|B|$ reductions. The green bars denote the number of PB, for which their being inside the MP is clearly supported by the energetic particle data (see Figure 2.A6 and related discussion above); black bars depict the number of the external $|B|$ -reductions with clearly dominating soft energetic particles from the MSH. We note that in $\sim 15\%$ cases the soft-energetic particle data were absent and that, if the trapped energetic particles were seen just inside the MP, their intensity usually exceeded that in the MSH. Fewer energetic particles in the OT could be due to particle leakage into the downflowing MSH, while in the PB they are back-scattered by the stronger TBL at the PB outer border.

All in all, Figure 2.4 shows the OT being encountered for positive tilts and the PB at negative tilts. Specifically, the maximum of 20 PB cases occurs for tilts between -15° and -25° , and 77% of the PB are registered at tilts $< -5^\circ$; 6 OT cases are seen at negative tilts and 21 cases at positive tilts ($> |5^\circ|$). The energetic particle data prove that the PB occurs on closed magnetic field lines in a majority of cases (e.g., in 63% for tilts between -15° and -25°). No clear dependence of PB occurrence on magnetic shear across the MP has been found, while for $> 65\%$ cases the IMF $B_z > 0$.

As mentioned in the discussion of Figure 3, the high-beta (2–15) plasma and direct interaction with the incident MSH flows are distinct differences of the PB from the rest of the outer cusp. Generally in the OC, quasi-

perpendicular MSH ions are strongly guided by the magnetic field (Kirpichev et al., 1999). The domination of PB during IMF $B_z > 0$ can be accounted for as follows: (i) during southern IMF the minimum $|B|$ in the OC is shifted equatorward (cf. Spreiter and Briggs, 1962, Maynard, 2003), and that favors penetration of the MSH flows into the cusp throat; (ii) drifts, caused by the inductive electric field from the MSH, move plasma from the PB towards the plasma sheet for IMF $B_z < 0$, and from the tail boundary layer towards the PB for $B_z > 0$. Quasi-perpendicular ions, evident up to the upper energy limit in Figure 6.B4c, and electrons are trapped in the diamagnetic cavity.

We infer their local heating by the strong turbulence (see, e.g., Savin et al., 1998b) both from continuous ion distributions (from MSH energies up to soft energetic particle energies) and from their absence outside the PB deeper in magnetosphere. Particles from the plasma sheet can also contribute to the trapped population (Shabansky and Antonova, 1968), but, for that to happen, they should lose their parallel momentum excess by wave-particle interactions in the TBL (i.e. be back-scattered into the PB by nonlinear waves in the TBL).

5. Discussion

After presentation of data for the characteristic case of 19 June 1998 from Interball-1 and Polar, and a statistical study of perturbations near the high-latitude MP, we discuss the data presented earlier. Savin et al. (1998b, 2001, 2002a, b, 2004) and Maynard (2003) provide relevant references and results.

5.1. TURBULENT BOUNDARY LAYER AND MULTISCALE RECONNECTION

An inspection of the TBL crossings observed by Interball-1 (Figure 2.A1–2.A3) shows that on 19 June 1998 the TBL is registered at a rather typical position (see Sections 2–3). The TBL is concentrated at high latitudes ($|Z| > 4 R_E$) over the cusp and downstream of it. Savin et al. (2002a) demonstrated that a substantial part of the events in the tail ‘wings’ at the higher latitudes is independent on the IMF B_y , which contradicts the ‘sash’ predictions (Maynard et al., 2001). Approximately another half of the ‘wing’ events follows the ‘sash’ B_y -dependence. Another possible ‘wing’ source is the TBL downstream of the cusps (see Figure 1, and Savin et al., 2004). The presence of TBL ‘wings’ for any IMF B_y is in agreement with the MSH plasma penetration not only in the cusp-shaped dayside and ‘sash’ regions, but on the tail flanks (cf. Haerendel, 1978). The TBL is present in $> 80\%$ of the high-latitude MP crossings. The most intense events could be approximated by effective disk with diameter of $\sim 6 R_E$ above the dayside cusps, with an average maximum

RMS of about $22nT$ (see Savin et al., 1999). At low latitudes the intense events are encountered mostly in the tail.

For positive tilts, the TBL is indented in the YZ -plane (Figure 2.2). This agrees with the direct interaction of the open cusp throat with the incident MSH flows (Figure 1). The indentation in the TBL/MP does not represent a characteristic feature of the winter hemisphere (Figure 2.2). This asymmetry suggests that the interaction of the MSH flow is different for negative and positive tilts (see Figure 6.B7). No such crucial dependence has been found for the IMF direction, while specific shifts have been outlined, for example by Merka et al. (2000).

Essential MSH plasma heating (~ 300 eV) occurs in 82% of the cases within the TBL ‘diamagnetic bubbles’ (Savin et al., 1999). The correlation of soft energetic particles with strong turbulence has been confirmed by the Interball-1 and Polar data on 19 June 1998 (see Section 2.4 and Chen and Fritz, 1997, Blecki et al., 1998, Savin et al., 2002c). The presence or lack of energetic particles also helps in placing of the PB and OT inside or outside the MP (see also Section 5.2 below). Detailed pitch-angle distributions and energy cuts point to three different populations of energetic particles in the disturbed TBL outside the MT: (i) dense, heated MSH particles (< 50 keV), which constitute a source for the soft energetic ions in PB (see panel a in Figure 6.B4, Figure 7 and related discussions in Section 2.4); (ii) intermediate energy particles escaping from PB; (iii) bursty higher energy perpendicular ions, presumably locally accelerated by the wide-band turbulence. In the PB the loss-cones in ion distributions with energies of 7–25 keV directed towards the nearest (southern) ionosphere conform to the PB as a source for precipitating particles into the dayside cusp ionosphere. On 19 June 1998, the data display typical TBL features (Figure 2.A6 and 6.A6): these are (i) wideband intensive nonlinear fluctuations (with energy density up to 40% of kinetic plasma energy density in flowing MSH); (ii) ‘diamagnetic bubbles’ with $|B|$ drops from $\sim 75nT$ down to few nT (Figure 6.B6), and (iii) plasma heating and field-aligned jets, etc. (cf. Savin et al., 1998b, 2002a, b, Sandahl et al., 2002). The latter has been accounted for by reconnection bulges at the border of the outer cusp (Dubinin et al., 2002, Savin et al., 2002a, 2002b, 2004).

To combine these with well-known reconnection for northward IMF downstream of the cusp for a smooth MP, we propose the scheme depicted in Figure 8. On the indented MT in the open cusp throat (cf. Figures 1b and 6.B7) there are at least two places with anti-parallel magnetic fields on the MP. The upper reconnection site is the ‘standard’ large-scale (few R_E) tail reconnection, the lower one is inside the OT, superimposed on the TBL fluctuations. The original magnetospheric field lines are marked by the lines with arrows and those of the IMF by lines with circles. Reconnection pulses inside the OT can be recognized in Figure 6.B6: the local magnetic field is

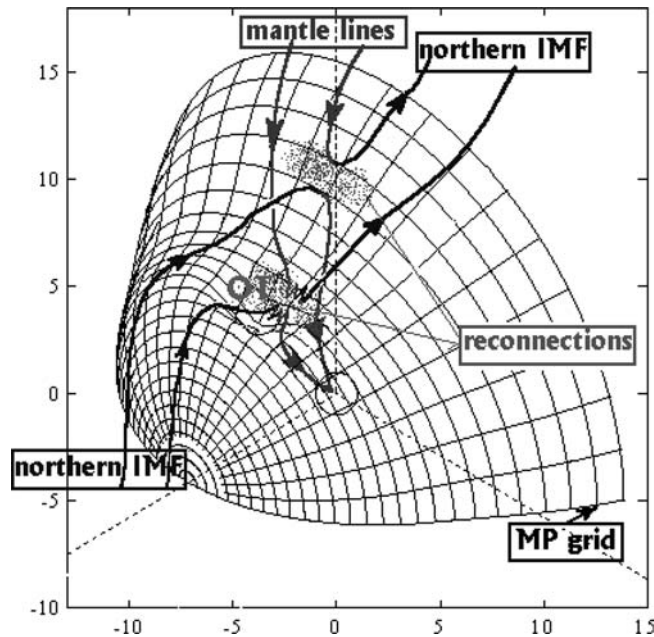


Figure 8. Sketch for multiple reconnection sites at the indented MP for a northern IMF.

practically anti-parallel (see changes in B_y), and the dominant positive V_y -burst direction corresponds to magnetic stress (Dubinin et al., 2002). However, the comparison with the SW data from Geotail via GDCF obviously demonstrates no evidence for the SW driving of the plasma jets. Instead, the jets' repetition conforms to TBL-driving (see Figure 2.A5, A6 and related discussions in Section 2). Savin et al. (2002a) accounted for the difference of the power for Polar and Interball spectra of about one order of magnitude by the average magnetic field annihilation in a patchy reconnection (cf. Maynard, 2003). Similar reasoning for 29 May 1996 has been proposed by Savin et al. (2004).

Simultaneously, Figure 6.B6 demonstrates the dominance of the jet ion energy over the magnetic energy, that invokes triggering of the reconnection by the accelerated plasma jets that originated in the upstream TBL (see Figure 2.6, Figure 4 and related discussions). This bursty reconnection corresponds to smaller (middle) scales. Later on we refer to this as 'primary cusp reconnection'. Its characteristic scale is estimated as a few thousand km. The primary cusp reconnection differs from that at low latitudes, where the MSH dynamic pressure results first in a compression of the static magnetic field and then a release of the magnetic energy through the (large-scale) reconnection into plasma acceleration and heating. At high latitudes the TBL-triggered bursty reconnection plays the role of a 'shutter', which provides the local

transformation of the MSH kinetic energy directly into that of deflected/accelerated flows. Savin et al., (2002a) give the respective picture for the southern IMF, which is confirmed by the sunward/vertical flows measured in the cusp vicinity by Magion 4. Maynard et al. (2003a,b) provides further evidence for most of the merging being at high latitudes and being unsteady; multiple sites can be operative at once and active for 30 s to a few minutes. In a sense, merging is continuously happening, but not continuously at most sites.

Savin et al. (2004) demonstrate parallel operation of the primary cusp reconnection and remote laminar reconnection tailward the cusp on 29 May 1996 for the dominant IMF $B_z > 0$. Belmont and Rezeau (2001) show that strong ULF fluctuations near the MP can independently result in micro-reconnection all along the MP. Another possibility is that the secondary reconnection of the fluctuating fields in the TBL can provide the plasma inflow even for a quasi-parallel magnetic field (cf. Chandler et al., 1999). The micro-reconnection scales range down to an ion gyroradius. The fluctuations (including micro-reconnection) create the specific structure of the MP current sheet (s) with magnetic islands, which results in plasma percolation through the nonlinear boundary network (Kuznetsova and Zelenyi, 1990). An estimate shows that this stochastic plasma transfer through the TBL/cusp walls can populate both the cusp and low latitude boundary layer; the diffusion coefficient $D_p \sim (5-10) 10^9$ m/s for typical MP parameters results in a particle influx of $(1-2) 10^{27}$ particles/s (Savin et al., 1999). Primary cusp reconnection should certainly amplify the plasma inflow.

Comparison with the kinetic simulation of thin current sheets (Savin et al., 2002b) demonstrates that the general spectral and bi-spectral properties of the TBL fluctuations can be reproduced by the modeling. For example, the registered quasi-coherent structures can be regarded as residuals of the nonlinear evolution of current sheets; the ‘diamagnetic bubble’ presence supports this suggestion as the field depletions in the middle of equilibrium current sheets is reproduced by a number of modeling results of the nonlinear current states (see, e.g., Buechner et al., 1999 and La Belle-Hamer et al., 1995). As a result of the multi-scale reconnection, field lines are connected through the TBL in a statistical sense, without an opportunity to trace individual field lines in the inhomogeneous non-equilibrium 2-phase medium, one phase being the frozen-in ‘MHD’ plasma and another represented by the unmagnetized ‘diamagnetic bubbles’ embedded in the nonlinear current sheets and vortices. The latter ‘phase’ (in the statistical sense) provides the power-law spectra with slope ~ -1 (Savin et al., 2002b), which implies a special type of translation symmetry of the fluctuations. The quasi-coherent wave-packets are breaking the Gaussian statistics, most probably due to TBL intermittency.

5.2. PERTURBATION OF MAGNETOSHEATH FLOWS BY THE OUTER CUSP THROAT

We now address another primary mechanism for energy and mass transfer at the MSH/cusp interface: direct interaction of the MSH flow with the outer cusp. From Figure 1, 2, 2.A1–2.A3, 2.A6 and 6.B6–6.B7, we can see that the cusp throat might present a substantial obstacle to the plasma flow streaming around the MP. In the zero approximation the magnetic barrier can be regarded as a rigid local obstacle, the large-scale laminar reconnection being inferred as a primary mechanism for the mass and energy transfer inside the MP (see, e.g., Russell (1995), Maynard (2003), and references therein). The interaction with the barrier occurs at low latitudes and in region “1” in Figure 1 (at positive tilts). In the plasma–plasma interaction in the high-beta case over the cusp throat (at negative tilts, see Figure 3) only high-amplitude waves and, probably, surface charge at the MP can constitute the means for interactions in a self-consistent regime with pre-existed high-beta stagnant plasma (see Section 5.3 and Lavraud et al., 2002). The local plasma–plasma interaction occurs also at the interface of the OT and MSH, but its intensity should be smaller as the turbulence has its maximum magnitude deeper in the throat at the OT/OC transition.

Multi-point data on 27 January 1997 permit the TBL depth in the near tail to be evaluated as being $\sim 2 R_E$ from the satellite–subsatellite measurement comparisons (Savin et al., 2004). The high-latitude interactions result in the substantial MSH kinetic energy transformation into thermal energy of the particles: the ratio W_{kin}/nT_i rises from 20 to 50%. The schematic representation of the resulting picture is marked by “2” in Figure 1a. The sound Mach number in the unperturbed MSH ($M_s \sim 2$) drops to $M_s \sim 1$ downstream of the cusp obstacle. In the two cases described in Savin et al. (1998b), the MSH/OT transition in going through thin magnetic barriers has $B^2/2\mu_0 \sim nT_i + W_{\text{kin}}$ in both the MSH and OT. The latter does not resemble intermediate/slow shock solutions (see, e.g., Karimabadi et al., 1995).

$M_s \sim 2$ is also seen in the Interball-1 data just outside the MP on 29 May 1996 (Savin et al., 1998a, 2004). Savin et al. (2001) compared the maximum ion heating in the TBL on 2 April 1996 with the Rankine–Hugoniot predictions for shock transitions using a magnetosonic Mach number ($M_m \sim 1.2$) in the MSH, an Alfvénic Mach number for the normal ion speed ($M_{An} \sim 1.2$) upstream of the OT, and a full Alfvénic Mach number ($M_A \sim 3.5$): $T_i/T_{\text{MSH}} \sim 1 + \gamma - 1)M^2 \sim 1.6$ and ~ 5 , respectively, for the Alfvénic Mach numbers of 1.2 and 3.5; we take $\gamma \sim 5/3$, and take into account that $nT_i \gg W_{\text{kin}}$ in the OT. The experimental ion temperature gain on those days of ~ 2.2 is higher than it should be at the inclined shock transition, but it is still much less than the maximum heating at the perpendicular shock. Thus Savin et al. (2001) concluded that the energy transformation in the TBL significantly differs from a thin shock transition.

Similarly, the disturbed region at 09:45–10:00 UT (Figure 2.6) should be treated as a unique ‘thick’ region with both remotely operated ion velocity and pressure cascades and local discontinuities (e.g., MP and a boundary at ~09 UT). The presence of the bursty super-Alfvénic flows in the upstream TBL and PB (see discussion of the jet at 09 UT in Section 2.2) obviously contradicts the MHD descriptions of thin shocks. We would like to point out also that the TBL provides secondary magnetic flux reconnection at any magnetic shear. The magnetic flux, reconnected at small scales, on average, is capable of driving magnetospheric convection (Haerendel, 1978).

At this point we touch an open critical problem of the SW/magnetosphere interaction: where are the geomagnetic field lines being opened? Our current understanding is that this process is both a multi-point and a multi-scale one. We believe that the MSH/cusp interface plays the dominant role in the opening of flux tubes, at least during quasi-steady conditions. The tilt angle dependence of the cusp position both at high and low altitudes (Merka et al., 2000) has a natural explanation if the TBL is a general source of plasma for the cusps: (a) the higher the tilt (i.e. the closer the dipole axis points to the Sun), the more open the OT becomes to the external MSH flow (i.e. the OT tailward wall represents a steeper obstacle for the MSH flow); (b) the higher the shift/penetrations at the OT tailward wall, the deeper the MSH plasma will be seen on the tail field lines; and (c) the deeper the plasma penetration (and/or tailward field line deflection), the more tailward it will be projected into the polar cap (i.e. the cusp is at higher invariant latitudes). Note that the tilt-related cusp shift has no explanation in the ‘traditional’ global-reconnection approach. At anti-sunward dipole tilts Interball detects demagnetized heated plasma of MSH origin in ‘plasma balls’, which have scales of a few R_E , on the Earthward side of the MP. The thick multilayered structure implies a type of interconnected non-equilibrium boundary, and the PB represents a local obstacle (partially absorbing) for the incident MSH flow. The observed high-amplitude waves constitute the means for their interaction.

The large-scale PB can have substantial impact on the MSH/magnetosphere interactions as a storage of MSH plasma, which in turn becomes a source of the MSH plasma to the magnetosphere. A sunward tilt opens the OT for direct interaction with the MSH flow. The asymmetric streamlining of the MSH flow around cusps is shown in Figure 6.B7: in summer, the MSH flow produces a TBL over the outer cusp, whereas in winter the TBL is located both upstream of the MP and at the outer PB border. The general difference of the OT with the $|B|$ reductions (Figure 6.B5) from a PB is that the MP, while being imbedded into strong perturbations, effectively isolates the MSH electrons and most of ions from the magnetosphere in the OT case. The energetic particle data prove the PB closed topology in a majority of the cases. The probability of crossing the PB at GSM $|Z| > 4$

R_E at tilts $< -5^\circ$ is $\sim 25\%$. Thus, the PB are present rather regularly in the outer cusp at the negative tilts, and they could provide a valuable contribution in the populating of the magnetosphere by MSH plasma. They could also store soft energetic particles in the minimum- $|B|$ configuration (cf. Sections 2.5, 5.1 and Shabansky and Antonova, 1968). MHD modeling (Maynard et al., 2003b) demonstrates that low- $|B|$ regions occur at negative tilts in the cusp vicinity inside the dayside MP, thus confirming that the PB are a necessary element of global equilibrium at the magnetospheric boundary.

5.3. TURBULENCE SOURCES AND PROPERTIES

Following Haerendel (1978), we suppose that first of all the TBL results from the turbulent mixing driven by the regular MSH flow interaction with the near-cusp magnetopause. The disturbed flows, accelerated in a region remote from the cusp reconnection site, can contribute to the TBL generation as well. The large-scale ‘remote’ reconnection sites (see Section 5.1) also regulate the TBL position by shifting the MP indentation according to the SW parameters. Away from the plasma stagnation region in the OT center, the Kelvin–Helmholtz plasma vortices with secondary reconnections should provide a mechanism for plasma heating/transport (cf. Q. Chen et al., 1997). The fluctuation level in the MSH, especially downstream of quasi-parallel bow shocks, is believed to stimulate the generation of ULF turbulence in the TBL.

Savin et al. (2004) reported that the correlation for time intervals of ~ 5 – 15 min in the post-BS region, middle MSH and OT reaches 0.6–0.7, and is a manifestation of the TBL/MP reactions to the SW/MSH transients. Thus, the transient current sheets and density gradients generated by dynamic SW interactions with the MP should contribute to turbulence in the TBL. However, simultaneous Geotail spectra and correlation analysis suggest the local character of the main TBL disturbances (Figure 2.A5–2.A6 and 6.B6). As a whole, the TBL collects, transforms and generates the plasma flow and magnetic field disturbances simultaneously from several sources. Its status depends on the short-term time history of the SW/magnetosphere interactions, influencing, in turn, the interaction of the magnetosphere with newly-arriving disturbances at each particular moment.

Simultaneous Interball/Polar data demonstrate the presence of a maximum at 1–2 mHz throughout the TBL in both hemispheres. The spectra of W_{kin} and nT_i (Figure 2.A6, Figure 4) allow this disturbance to be traced throughout the MSH. Besides the transient/dynamic reactions of the TBL to external disturbances, the TBL appears to have well-defined inherent properties, which have been traced at different points of the MSH and MP boundary layers during the favorable period of relatively steady SW

parameters. The modern wavelet technique provides us with strong evidence that the spectral characteristics of the TBL in the different hemispheres on 19 June 1998 are well defined. The most pronounced TBL waves at 0.003–0.5 Hz have characteristic kinked shapes and slopes (Savin et al., 2002a). We have checked the waves in the TBL on 26 August 1995, 29 May 1996, and 23 June 1998 and found that the kinked shape with slopes of 1–1.5 and 2–2.6 are characteristic for the TBL. The higher value of the slope in the TBL of ~ 2 is close to that characteristic for the developed self-consistent kinetic turbulence in the geomagnetic tail (see, e.g., Zelenyi and Milovanov, 1998, and references therein).

Comparison with the simulation of thin current sheets provides evidence that the random current sheets with features of coherent wave-packet can result in slopes of ~ -1 in the magnetic power spectra (see Section 5.1 and Savin et al., 2002b). Savin et al. (2001) have proposed the following self-consistent concept of TBL interactions. Cascade-like wavelet and bicoherence spectrograms and the wavelet correlation time suggest a coherent, most probably 3-wave, interaction between wave trains, while the disturbances seem to be random in waveforms.

The local wave trains originate from the interaction of the disturbed MSH flows with the MP; their dispersion is indicative of kinetic Alfvén waves (KAW, see Stasiewicz et al., 2001, and Savin et al., 2004). Johnson and Cheng (1997) proposed excitation of the transverse KAW at the MP by the interaction of compressible MSH waves with the current sheet; the wave properties discussed above are in satisfactory agreement with their predictions. Later Belmont and Rezeau (2001) demonstrated the growth of the trapped large-amplitude KAW inside the non-uniform current sheets. Our new finding here from the ion fluctuations is the global (over the MSH) synchronization at ~ 1.3 mHz. The MSH synchronization is seen mostly in the density (MS) fluctuations, which are transformed into velocity (KAW) fluctuations in the upstream TBL (Figure 6.B1–6.B3). Turning back to the TBL interaction scheme, while linear KAW resonances (i.e. singularities in the equations of Belmont and Rezeau, 2001) are absent, we suggest that the coherent large-scale structures can originate from the reverse KAW cascades, focused by the concave MP and/or cusp walls in the outer cusp vicinity (cf. Figure 2.A6, 6.B1–6.B4 and Savin et al., 2001, 2004). At the nonlinear stage the Alfvénic disturbances in the TBL modulate the incident MSH flow in a self-consistent manner, being globally synchronized by phase coupling with the large-scale variations (at ~ 3 –5 mHz, see Figure 2.A6, Figure 4 and Savin et al., 2003a).

Thus, the chain is closed: the TBL seems to be a ‘thick’ multi-scale self-organized system of interacting nonlinear waves. This suggests a qualitative difference from the traditional approach when the MSH/cusp interaction is regarded as a linear superposition of magnetospheric responses to SW or MSH disturbances. Note also that the long-term correlation is sug-

gestive of systems out of equilibrium near the critical point (cf. Consolini and Lui, 2000). The kinked TBL spectra with characteristic slopes remarkably resemble those in the near-Earth neutral sheet in the state of self-organized criticality (see, e.g., Zelenyi and Milovanov, 1998). Using $f_1 + f_2 \sim f_3 = 4.5$ mHz $\sim k\bar{V}/2\pi$ (see Figure 6.3B in Section 4.2 and related discussions) as a proxy for evaluation of the characteristic scale, we obtain $L \sim V_{\text{MSH}} / f_3 \sim 5\text{--}7 R_E$. This is comparable with the TBL span along the MP in the indentation or with that of a ‘plasma ball’ (Figure 6.B7). On the other hand, the spectral maximum seen in the MSH, through the TBL and into the outer cusp (see Figure 6.B1 and 6.B2) demonstrates the global character of the phenomenon. Such long waves can pass through the MP (see Figure 6.B2) and might resonate with the dayside flux tubes in the Pc 4–5 range or at higher harmonics (cf. Pilipenko et al., 1999).

The general scheme presented above has been defined concretely in Section 2.2 for the low-shear MP in front of the PB. As mentioned above it is valuable both because of different types of plasma–plasma interaction (versus a plasma–magnetic barrier interaction at the low-latitude MP) and because the resulting PB inside the MP represents a great MSH plasma reservoir for the inner magnetosphere. The main mechanism for the plasma–plasma (i.e. MSH flow with PB) interaction is via the nonlinear waves in the TBL upstream of the MP in the flowing MSH, but has been poorly studied at high latitudes. The main physical problem is that the practically demagnetized PB (ion beta ~ 15) cannot interact with the flow via magnetic forces this constitutes the principal difference with the dayside low-latitude MP which is generally a magnetic barrier.

We have analyzed the detailed dynamics of the ion energy and of the Poynting flux to clarify further the pattern of interactions in the upstream TBL. The wave packets, propagating upstream from the MP, stimulate partial randomization of the flow far in front of MP (>1 h). The interaction of fluctuations in the incident flow with the upstream-propagating waves launches transient perturbations downstream, which both result in magnetosonic jets (Figure 2 and 3) and trigger the cascade-like nonlinear energy transformation in the TBL. This causes the MSH kinetic energy to drop by up to 40%, while the jets transport the ion momentum excess downstream. The drop of kinetic energy results also in the amplification of low-frequency pulsations (at ~ 1.3 mHz). These fluctuations are phase-coupled with the spectral maxima at 3–10 mHz at $\sim 09:00$, $09:15$, $09:30$ and $09:45$ UT in Figures 2.A6, 6.B 1, and 6.B2. A macro-equilibrium cannot be achieved in the outer BL until several characteristic periods have elapsed, which correspond to the time scales of patchy merging in ionosphere (Maynard, 2003). The strong upstream fluctuations plasma density and velocity can be visible at the lower latitudes (cf. ‘slow mode transitions’, Song et al., 1992).

5.4. CONCLUDING REMARKS

The results of our data analysis strongly indicate that the TBL fluctuations, instead of being random, are phase-coupled and ‘organized’ into cascades of nonlinear (presumably 3-wave) interactions. The coherent waves described above control the spectral shape, and result in non-Gaussian statistical characteristics of the disturbances that conforms to the fluctuation intermittency (Savin et al., 2002b).

We suggest that, in the SW energy transformation to the magnetosphere, multi-scale TBL processes play at least a comparable role to those of large-scale reconnection, which generally occurs far from the cusp. Turbulent diffusion and percolation are capable of populating the magnetosphere with MSH plasma. The TBL transforms the MSH flow energy, including deceleration and heating of the flow downstream from the high latitude cusp. Patchy time-varying reconnection provides the means for energy conversion and plasma transport in the small-scale portion of the TBL energy cascade.

The plasma–plasma interaction over the closed cusp throat operates via reflected waves, which provoke the chaotization of ~40% of the upstream kinetic energy. The characteristic flow decay into magnetosonic/Alfvénic streams also launches TBL nonlinear cascades. This represents the non-stationary non-MHD mechanism for the momentum loss via TBL vortex streets, which diminish the effective plasma–plasma friction similar to that in plasma–plasma hydrodynamics (cf. Haerendel, 1978). The magnetosonic jets carry the flow momentum ‘excess’ downstream, permitting deceleration of the rest of the boundary layer plasma.

Acknowledgements

We thank K. W. Ogilvie and the SWE team for providing WIND solar wind dynamic pressure data, R. Lepping for providing WIND magnetic field data, J. Scudder for providing the HYDRA data and S. Lamey for help in preparation of the paper. We thank the GEOTAIL/MGF team, especially H. Matsui, for providing high-resolution magnetic field data used in this paper. This work was partially supported by International Space Science Institute, European Commission Research Training Network HPRN-CT-2001-00314, and by grants KBN 4 T12 016 28, INTAS 03-50-4872, RFFR 02-02-17160 and 03-02-16967, Science School 1739 2003 2.

References

- Belmont, G., and Rezeau, L.: 2001. “Magnetopause Reconnection Induced by Hall-NIED Fluctuations”, *J. Geophys. Res.* **106**(A6), 10,751–10,760.

- Blecki, J., Rothkaehl, H., Kossacki, K., Wronowski, R., Klos, Z., Juchniewicz, J., Savin, S., Romanov, S., Klimov, S., Triska, P., Smilauer, J., Simunek, J., Kudela, K., and Forster, M.: 1998. "ULF-ELF-VLF-HF Plasma Wave Observations in the Polar Cusp Onboard High and Low Altitude Satellites", *Phys. Scripta* **75**, 259–263.
- Büchner, J.: 1999. "Reconnection: Space Plasma Simulations for Multi-Spacecraft Satellite Observations in the ISTP era", *Phys. Chem. Earth* **24**, 179–187.
- Chandler, M. O., Fuselier, S. A., Lockwood, M., and Moore, T. E.: 1999. "Evidence of Component Merging Equatorward of the Cusp", *J. Geophys. Res.* **104**, 22,623–22,633.
- Chen, J., Fritz, T. A., Sheldon, R. B., Spence, H. E., Spjeldvik, W. N., Fennell, J. F., Livi, S., Russell, C. T., Pickett, J. S., and Gurnett, D. A.: 1998. "Cusp Energetic Particle Events: Implications for a Major Acceleration Region of the Magnetosphere", *J. Geophys. Res.* **103**, 69–78 .
- Chen, J., and Fritz, T. A.: 1998. "Correlation of Cusp MeV Helium with Turbulent ULF Power Spectra and its Implications", *Geophys. Res. Lett.* **25**, 4113–4116 .
- Chen, Q., Otto, A., and Lee, L. C.: 1997. "Tearing instability, Kelvin–Helmholtz Instability and Magnetic Reconnection", *J. Geophys. Res.* **102**(A1), 151–161 .
- Chen, S.-H., Boardsen, S. A., Fung, S.F., Green, J. L., Kessel, R. L., Tan, L. C., Eastman, T. E., and Craven, J. D.: 1997. "Exterior and Interior Polar Cusps: Observations from Hawkeye", *J. Geophys. Res.* **102**(A6), 11,335–11,347.
- Consolini, G., and Lui, A. T.: 2000. "Symmetry Breaking and Nonlinear Wave–Wave Interaction in Current Disruption: Possible Evidence for a Phase Transition", in R. Fujii, M. Hesse, R. Lysak, and S. Ohtani (eds.), *Magnetospheric Current Systems, Geophysical Monograph 118*, American Geophysical Union, Washington D.C., pp. 395–401.
- Dublihin, E., Skalsky, A., Song, P., Savin, S., Kozyra, J., Moore, T. E., Russell, C. T., Chandler, M. O., Fedorov, A., Avakov, L., Sauvaud, J. A., and Friedel, R. H. W.: 2002. "Polar-Interball Coordinated Observations of Plasma Characteristics in the Region of the Northern and Southern Distant Cusps", *J. Geophys. Res.* **107**(A5), 1010.29/2001 JA900068.
- Fritz, T. A., Chen, J., and Sheldon, R. B.: 1997. "The Role of the Cusp as a Source for Magnetospheric Particles: A New Paradigm?", *Adv. Space Res.* **25**, 1445–1457 .
- Haerendel, G., and Paschmann, G.: 1975. "Entry of Solar Wind Plasma into the Magnetosphere", in B. Hultqvist, and L. Stenfl (eds.), *jem Physics of the Hot Plasma in the Magnetosphere*, Plenum, NY, pp. 23.
- Haerendel, G.: 1978. "Microscopic Plasma Processes Related to Reconnection", *J. Atmos. Terr. Phys.* **40**, 343–353.
- Johnson, J. R., and Cheng, C. Z.: 1997. "Kinetic Alfvén Waves and Plasma Transport at the Magnetopause", *Geophys. Res. Lett.* **24**, 1423–1426.
- Kirpichev, I., Fedorov, A., Grigoryev, A., Budnick, E., and Dubinin, E.: 1999. "Quasi-trapping of the Charged Particles in the Local Minimum of Magnetic Field in Exterior Cusp", *Cosmic Res. (Russia)* **37**(6), 638–643.
- Klimov, S. I., Nozdrachev, M. N., Triska, P., Voita, Ia., and Galeev, A. A.: 1986. "Investigation of Plasma Waves by Combined Wave Diagnostic Device BUDWAR PROGNOZ-10-INTERCOSMOS", *Cosmic Research (Transl. from Russian)* **24**, 177–184.
- Kuznetsova, M. M. and Zelenyi, L. M.: 1990, "The Theory of FTE: Stochastic Percolation Model". in C. T. Russell, E. R. Priest and L. C. Lee (eds), *Physics of Magnetic Flux Ropes*, pp 473–488 American Geophysical Union..
- La Belle-Hamer, A. L., Otto, A., and Lee, L. C.: 1995. "Magnetic Reconnection in the Presence of Sheared Flow and Density Asymmetry: Application to the Earth's Magnetopause", *J. Geophys. Res.* **100**, 11,875–11,889.

- Lavraud, B., Dunlop, M. W., Phan, T. D., Reme, H., Bosqued, J. M., Dandouras, I., Sauvaud, J. A., Lundin, R., Taylor, M. G. G. T., Cargill, P. J., Mazelle, C., Escoubet, C. P., Carlson, C. W., McFadden, J. P., Parks, G. K., Moebius, E., Kistler, L. M., Bavassano-Cattaneo, M. B., Korth, A., Klecker, B. and Balogh, A.: 2002, "Cluster Observations of the Exterior Cusp and its Surrounding Boundaries Under Northward IMF". *Geophys. Res. Lett.* **29**(20), Art.No. (1995) Oct. 15.
- Maynard, N. C., Savin, S., Erickson, G. M., Kawano, H., Nemecek, Z., Peterson, W. K., Safranokova, J., Sandahl, I., Scudder, J. D., Siscoe, G. L., Sonnerup, B. U. O., Weimer, D. R., White, W. W., and Wilson, G. R.: 2001. "Observation of the Magnetospheric 'sash' and its Implications Relative to Solar-Wind/Magnetospheric Coupling: A Multisatellite Event Analysis", *J. Geophys. Res.* **106**, 6097–6122.
- Maynard, N. C.: 2003, "Coupling of the Solar-Wind/IMF to the Ionosphere Through the High Latitude Cusps" *Surveys in Geophysics* 25, this issue.
- Merka, J., Safranokova, J., Nemecek, Z., Fedorov, A., Borodkova, N., Savin, S., and Skalsky, A.: 2000. "High Altitude Cusp: INTERBALL Observations", *Adv. Space Res.* **25**(7/8), 1425–1434.
- Paschmann, G., Haerendel, G., Scopke, N., Rosenbauer, H., and Hedgecock, P. C.: 1976. "Plasma and Magnetic Field Characteristics of the Distant Polar Cusp Near Local Noon: The Entry Layer", *J. Geophys. Res.* **81**, 2883–2899.
- Petrinec, S. M., and Russell, C. T.: 1995. "An Examination of the Effect of Dipole Tilt Angle and Cusp Regions on the Shape of the Dayside Magnetopause", *J. Geophys. Res.* **100**, 9559–9566.
- Pilipenko, V., Fedorov, E., Mazur, N., Engebretson, M. J., and Hughes, W. J.: 1999. "Magnetohydrodynamic Waveguide/Resonator for Pc3 ULF Pulsations at Cusp Latitudes", *Earth Planets Space* **51**, 441–448.
- Pottelette, R., Malingre, M., Dulouloz, N., Apanicio, B., Lundin, R., Holmgren, G., and Marklund, G.: 1990. "High Frequency Waves in the Cusp/Cleft Regions", *J. Geophys. Res.* **95**, 5957–5971.
- Romanov, V., Savin, S., Klimov, S., Romanov, S., Yermolaev, Yu., Blecki, J., and Wronowski, R.: 1999. "Magnetic Turbulence at the Magnetopause: Plasma Penetration", *J. Tech. Phys. (Poland)* **40**(1), 329–332.
- Russell, C. T.: 1995, "The Structure of the Magnetopause", in: P. Song, B. U. O. Sonnerup and M. F. Thomsen (eds), *Physics of the Magnetopause*, American Geophysical Union, pp 81–98.
- Sandahl, I.: 2002. "Recent Cusp and Cleft Results from Interball", *Adv. Space Res.* **30**(7), 1711–1723.
- Savin, S. R.: 1994 "ELF Waves Near the High Latitude Magnetopause". In: *Abstracts of AGU Chapman Conference on Physics of the Magnetopause*, March 14–18, 41.
- Savin, S. P., Balan, O., Borodkova, N., Budnik, E., Nikolaeva, N., Prokhorenko, V., Pulkkinen, T., Rybjeva, N., Safranokova, J., Sandahl, I., Amata, E., Auster, U., Bellucci, G., Blagau, A., Blecki, J., Buchner, J., Ciobanu, M., Dubinin, E., Yermolaev, Y., Echim, M., Fedorov, A., Formisano, V., Grard, R., Ivchenko, V., Jiricek, F., Juchniewicz, J., Klimov, S., Ko-repanov, V., Koskinen, H., Kudela, K., Lundin, R., Lutsenko, V., Marghitu, O., Nemecek, Z., Nikutowski, B., Nozdrachev, M., Orsini, S., Parrot, M., Petrukovich, A., Pissarenko, N., Romanov, S., Rauch, J., Rustenbach, J., Sauvaud, J. A., Sarris, E. T., Skalsky, A., Smilauer, J., Triska, P., Trotignon, J. G., Vojta, J., Zastenker, G., Zelenyi, L., Agafonov, Y., Grushin, V., Khrapchenkov, V., Prech, L., and Santolik, O.: 1997. "Interball Magnetotail Boundary Case Studies", *Adv. Space Res.* **19**, 993–1015.
- Savin, S. P., Romanov, S. A., Fedorov, A. O., Zelenyi, L., Klimov, S. I., Yerinolaev, Y. I., Budnik, E. Y., Nikolaeva, N. S., Russell, C. T., Zhou, X. W., Urquhart, A. L., and Reiff,

- P. H.: 1998a. "The Cusp/Magnetosheath Interface on May 29, 1996: Interball-1 and Polar Observations", *Geoph. Res. Lett.* **25**, 2963–2966.
- Savin, S. P., Borodkova, N. L., Budnik, E. Yu., Fedorov, A. O., Klimov, S. I., Nozdrachev, M. N., Morozova, E. I., Nikolaeva, N. S., Petrukovich, A. A., Pissarenko, N. F., Prokhorenko, V. I., Romanov, S. A., Skalsky, A. A., Yermolaev, Yu. I., Zastenker, G. N., Zelenyi, L. M., Triska, P., Amata, E., Blecki, J., Juchniewicz, J., Buchner, J., Ciobanu, M., Grard, R., Haerendel, G., Korepanov, V. E., Lundin, R., Sandahl, I., Eklund, U., Nemecek, Z., Safrankova, J., Sauvaud, J. A., Rustenbach, J., and Rauch, J. L.: 1998b. "Interball Tail Probe Measurements in Outer Cusp and Boundary Layers", in J. L. Horwitz, D. L. Gallagher, and W. K. Peterson (eds.), *Geospace Mass and Energy Flow: Results from the International Solar–Terrestrial Physics Program*, Geophysical Monograph 104. American Geophysical Union, Washington D.C., pp. 25–44.
- Savin, S., Zelenyi, L., Budnik, L., Borodkova, N., Fedorov, A., Nikolaeva, N., Nozdrachev, M., Romanov, S., Petrukovich, A., Yermolaev, Yu., Mukai, T., Kawano, H., Kokubun, S., Lundin, R., Sandahl, L., Russell, C. T., Maynard, N., Parks, G., Amata, E., Safrankova, J., Nemecek, Z., Blecki, J., Buchner, J., and Nikutowski, B.: 1998c. "Manifestations of Boundary Layer Dynamics in Substorm Activity, MultiSpacecraft-Study", in S. Kokubun, and Y. Kamide (eds.), *SUBSTORM-4, International Conference on Substorms-4', Lake Hamana, Japan: March 9–13, 1998*, Terra Scientific Publ. Co., Tokyo, pp. 125–30.
- Savin, S., Budnik, E., Nozdrachev, M., Romanov, V., Yermolaev, Y., Zelenyi, L., Blecki, J., Buchner, J., and Nikutowski, B.: 1999. "On the Plasma Turbulence and Transport at the Polar Cusp Outer Border", *Czechoslovak J. Phys.* **49**(4a), 679–693.
- Savin, S. P., Zelenyi, L. M., Romanov, S. A., Klimov, S. I., Skalsky, A. A., Galeev, A. A., Smirnov, V. N., Nozdrachev, M. N., Yermolaev, Y. I., Avakov, L. A., Amata, E., Blecki, J., Buchner, J., Nikutowski, B., Dubinin, E. M., Nemecek, Z., Safrankova, J., Pedersen, A., Rauch, J. L., Rustenbach, J., Sauvaud, J. A., Song, P., and Stasiewicz, K.: 2001. "Turbulent Boundary Layer at the Border of Geomagnetic Trap", *JETP Lett.* **74**(11), 547–551.
- Savin, S., Zelenyi, L., Maynard, N., Sandahl, L., Kawano, H., Russell, C. T., Romanov, S., Amata, E., Avakov, L., Blecki, J., Buchner, J., Consolini, G., Gustafsson, G., Klimov, S., Marcucci, F., Nemecek, Z., Nikutowski, B., Pickett, J., Rauch, J. L., Safrankova, J., Skalsky, A., Smirnov, V., Stasiewicz, K., Song, P., Trotignon, J. G., and Yermolaev, Y.: 2002a. "Multi-Spacecraft Tracing of Turbulent Boundary Layer", *Adv. Space Res.* **30**(12), 2821–2830.
- Savin, S., Buchner, J., Consolini, G., Nikutowski, B., Zelenyi, L., Amata, E., Auster, H. U., Blecki, J., Dubinin, E., Fornacon, K. H., Kawano, H., Klimov, S., Marcucci, F., Nemecek, Z., Pedersen, A., Rauch, J. L., Romanov, S., Safrankova, J., Sauvaud, J. A., Skalsky, A., Song, P., and Yermolaev, Y.: 2002b. "On the Properties of Turbulent Boundary Layer Over Polar Cusps", *Nonlinear Processes in Geophysics* **9**, 443–451.
- Savin, S., Blecki, J., Pissarenko, N., Lutsenko, V., Kirpichev, L., Budnik, E., Borodkova, N., Nozdrachev, M., Zelenyi, L., Romanov, V., Sandahl, I., Sauvaud, J. A., Buchner, J., Nikutowski, B., Gustafsson, G., Stasiewicz, K., and Korepanov, V.: 2002c. "Accelerated Particles from Turbulent Boundary Layer", *Adv. Space Res.* **30**(7), 1723–1730.
- Savin, S., Zelenyi, L., Romanov, S., Sandahl, I., Pickett, J., Amata, E., Avakov, L., Blecki, J., Budnik, E., Buchner, J., Cattell, C., Consolini, G., Fedder, J., Fuselier, S., Kawano, H., Klimov, S., Korepanov, V., Lagoutte, D., Marcucci, F., Mogilevsky, M., Nemecek, Z., Nikutowski, B., Nozdrachev, M., Parrot, M., Rauch, J., Romanov, V., Romantsova, T., Russell, C., Safrankova, J., Sauvaud, J., Skalsky, A., Smirnov, V., Stasiewicz, K.,

- Trotignon, J., and Yermolaev, Yu.: 2004. "Magnetosheath – Cusp Interface", *Ann. Geophys.* **22**((1), 183–212.
- Shabansky, V. P., and Antonova, A. E.: 1968. "Topology of Particle Drift Shells in the Earth's Magnetosphere", *Geomagnetism and Aeronomy* **8**, 844–859.
- Song, P., Russell, C. T., and Thomsen, M. F.: 1992. "Slow Mode Transition in the Frontside Slow Mode Transition in the Magnetosheath", *J. Geophys. Res.* **97**, 8295–8305.
- Song, P., Russell, C. T., Gombosi, T. I., Spreiter, J. R., Stahara, S. S., and Zhang, X. X.: 1999a. "On the Processes in the Terrestrial Magnetosheath, 1: Scheme Development", *J. Geophys. Res.* **104**, 22,345–22,355.
- Song, P., Russell, C. T., Zhang, X. X., Gombosi, T. I., Stahara, S. S., and Spreiter, J. R.: 1999b. "On the Processes in the Terrestrial Magnetosheath, 2: Case Study", *J. Geophys. Res.* **104**, 22,357–22,373.
- Spreiter, J. R., and Briggs, B. R.: 1962. "Theoretical Determination of the Form of the Boundary of the Solar Corpuscular Stream Produced by Interaction with the Magnetic Dipole Field of the Earth", *J. Geophys. Res.* **67**, 37–51.
- Stasiewicz, K., Seyler, C. E., Gustafsson, G., Pickett, J., and Popielawska, B.: 1997. "Magnetic Bubbles and Kinetic Alfvén Waves in the High-Latitude Magnetopause Boundary", *J. Geophys. Res.* **106**, 29,503–29,514 .
- Yamauchi, M., and Lundin, R.: 1997. "The Wave-Assisted Cusp Model: Comparison to Low-Latitude Observations", *Phys. Chem. Earth* **22**, 729–734.
- Zelenyi, L. M., and Milovanov, A. V.: 1998. "Multiscale Magnetic Structure of the Distant Tail: Self-Consistent Fractal Approach", in A. Nishida, and D. N. Baker (eds.), *New Perspectives on the Earth Magnetotail*, Geophysical Monograph 105, AGU, Washington D.C., pp. 321–338.